ABSTRACT

Title of Thesis: RESONANCE BASED LOW FREQUENCY SYNTHETIC JET ACTUATOR MODELING, DESIGN, AND TESING

Lynn M. Gravatt, Masters of Science, 2006

Thesis Directed by: Professor Alison Flatau
Department of Aerospace Engineering
University of Maryland

Synthetic Jet Actuators have been the topic of extensive study in the aerospace industry because of their ability to actively control flow over aerodynamic surfaces without discrete control surfaces such as a flap. One challenge has been to develop a low frequency, lightweight actuator that can provide large displacements. This study will discuss the modeling, design, manufacture, and testing of a bimorph piezo-composite actuator that will provide such displacements at low frequencies. The design employs two opposing benders that provide a piston-type motion. The initial goals of this study were to achieve 30 m/s out of the slot while maintaining the mechanical resonant frequency of the system at about 100 Hz.

RESONANCE BASED LOW FREQUENCY SYNTHETIC JET ACTUATOR

MODELING, DESIGN, AND TESING

By

Lynn M. Gravatt

Thesis submitted to the Faculty of the Graduate School of the
University of Maryland, College Park, in partial fulfillment
of the requirements for the degree of
Masters of Science
2006

Advisory Committee:
Professor Alison Flatau, Chair/Advisor
Professor Inderjit Chopra
Professor James E. Hubbard Jr

Dedication

To Mom and Dad

Acknowledgements

I would like to acknowledge all of the people and organizations that made the completion of this work possible. First and foremost, I would like to thank my advisor, Professor Alison Flatau. Without her advice and support the complete of this would not have been possible. Secondly, I would like to thank Dan Clingman for all if help in getting me started with smart structures. His help and wealth of knowledge allowed me get on the fast track to understanding synthetic jets. Also, thank you to Professor Jim Hubbard for making our weekly meeting a little more interesting! A big thank you to all of my fellow graduate students who gave me friendship, support, and an incredible pool of knowledge. These include Sandra Urgrina, Luke Twark, David Pullen, Beverly Beasley, Brandon Fitchett, Shane Jacobs and Enrico Sabelli. You kids rock da casa! Lastly, I would like to thank Ted Whitley and Boeing Phantom Works for their financial support. Their confidence in this technology was the driving force behind this research.

Table of Contents

List of Figures

Chapter 1: Introduction to Active Flow Control and Synthetic Jet Actuators

1.1 Active Flow Control Overview

Active flow control is a means of modifying the characteristics of a flow field in order to achieve a desired result, examples of which include delaying or accelerating transition of flow from laminar to turbulent, reducing drag and enhancing mixing.[1] As far as aerospace engineering is concerned, active flow control is generally used as a means of controlling boundary layer separation. On both fixed and rotary wing aircraft, separation is associated with losses via a decrease in lift, an increase in drag and pressure recovery losses. Currently, aircrafts employ the use of flaps, ailerons and slats as a means of controlling flow. Unfortunately these are complex, costly, cumbersome and heavy.[2] There are a number of alternative ways of actively controlling flow over an aerodynamic surface. These include suction, deforming surfaces, acoustic excitation, pulsed jets, steady blowing, plasma actuation and oscillatory blowing.[3]

The first of these alternative methods used for active flow control was suction. It was developed in an elementary sense by Prantle as far back as 1904. The idea behind suction is to remove decelerated fluid near a surface and deflect high-momentum fluid towards the surface. In wind tunnel tests, the effects of suction have proven to

be very promising; however, because of the complexity and overall power requirements of the system it is not a feasible option for modern day aircraft.[2]

A second method being studied for active flow control is deforming surfaces. This method uses smart materials and actuators to deform the shape of an airfoil such that the wing can constantly and rapidly adapt to changes in aerodynamic conditions. Chandrasekhara and Wilder[4] were able to show that changing the curvature of an airfoil's leading edge slowly was effective in boundary layer control. Unfortunately, for many aerospace situations where flow field characteristics are rapidly changing (such as on a helicopter rotor blade) the speed at which the airfoil deforms cannot keep up with the rapidly changing flow conditions.

The use of acoustic excitation has been studied as a means to control flow for over a half a decade. Collins[5] was able to show that placing a loud speaker downstream of an airfoil and controlling the output frequency, while increasing the sound pressure level to 124 db, could cause separated flow to become fully attached over the airfoil. A number of other studies have shown similar results. The major issue with this method of flow control is that all successful acoustic tests have only been run inside a wind tunnel where resonance interactions with the tunnel walls have contributed to the response. These tests are hard to duplicate in open air. The high acoustic levels needed for the control also make this option impractical.

Active flow control has also been attempted by introducing pulsed jets into the free stream. For a fully pulsed jet, fluid is injected into the free stream and is reduced to zero at the end of each pulsing cycle.[6] Many studies have shown that pulsed jets can be effective in delaying separation and suppressing stall. This is due to the increase in vorticity production that occurs with an impulsively started jet flow.[7]

An alternative to introducing pulsed jets into the free stream is to introduce steady blowing. The purpose of this is to inject additional momentum into the low momentum flow near this surface. This results in a delay of boundary layer separation. While not as effective as the pulsed jets (because of the vorticity increase associated with pulsed jets) steady blowing is a simple means of flow control because it can be done passively by the use of a slot that diverts air from the lower upstream surface to the upper downstream surface.[2]

One of the newest forms of active flow control is though the use of plasma actuators. These actuators consist of two electrodes separated by a dielectric material. When a high voltage is applied to the electrodes the air ionizes in the region with the highest electric potential. When in the presence of an electric field gradient, the ionized air (plasma) produces a body force on the ambient air. This force creates a virtual shape over the surface on which the actuator is placed. [31, 32]

Finally, the form employed for this research is the use of periodic excitation, also known as oscillatory blowing. Recent studies have shown that the combination of a

jet along with periodic motion is effective in boundary layer control because it both accelerates and regulates the generation of vortices.[8] The effectiveness of this method depends on a number of different parameters, which include the size and location of the blowing slot, the oscillatory blowing momentum coefficient, the frequency of the oscillatory blowing and of course the shape of the airfoil in question.[8] This brings us to how oscillatory blowing is used in a synthetic jet.

1.2 Synthetic Jet Overview

One way of achieving active flow control is through the use of synthetic jet actuators to create oscillatory blowing. A synthetic jet actuator is essentially a "zero-net-mass-transfer-flux" actuator. This means that the actuator can transfer momentum in and out of the system without adding or subtracting any mass. Typically, low momentum fluid is drawn into the chamber of the synthetic jet and is ejected into the free stream as a high momentum jet.[9] Figure 1.1 shows how a typical synthetic works. The synthetic jet has a vibrating membrane which changes the volume of the chamber and forces fluid in and out through the orifice.[10]

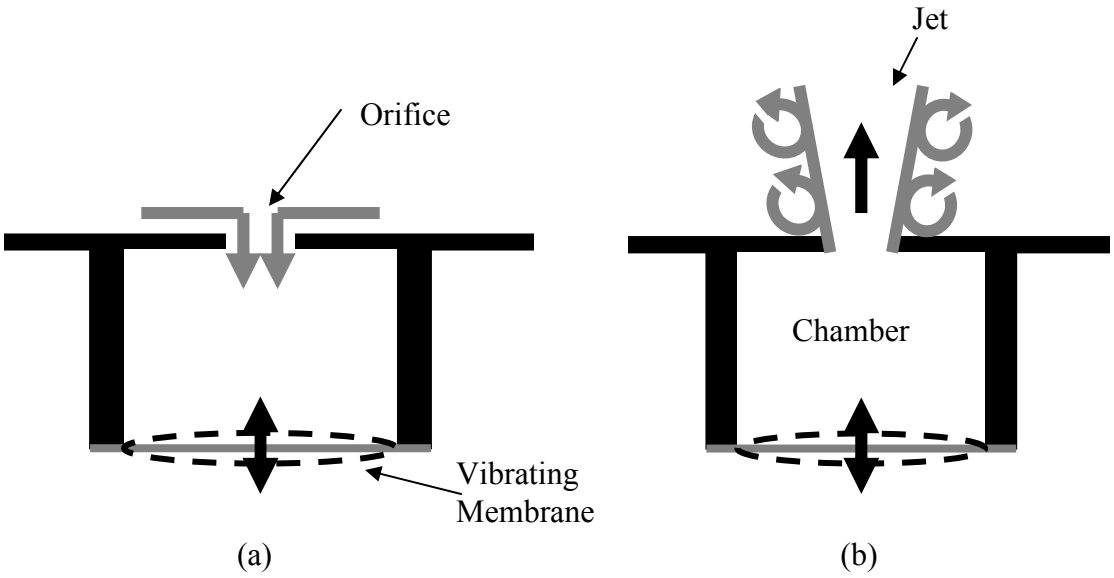

Figure 1.1 Synthetic jet actuator a) in flow b) out flow.[10]

In the previous section it was mentioned that the performance of a synthetic jet is quantified by two parameters. The first is the jet's oscillatory blowing momentum

coefficient, c_u. This is the ratio of the momentum imparted to the flow by actuation to the momentum in the free stream. The second is the dimensionless frequency of the jet, F^+. Equations 1.1 and 1.2 show the expressions for these two quantities:

$$c_u = 2(H/c)(U_j/U_\infty)^2 \tag{1.1}$$

$$F^+ = fx_f/U_\infty \tag{1.2}$$

where H is the synthetic jet slot height, c is the airfoil chord length, U_j is the velocity of the jet, U_∞ is the free stream velocity, f is the jet excitation frequency and x_f is the distance between the slot and the trailing edge of the airfoil or flap.[10]

In the case of this research, the vibrating membrane is a piezo electrically actuated membrane. Piezoelectric actuators are of interest for active flow control because they have a relatively high energy density and they are much smaller and weigh less than conventional actuators (such as electromechanical, hydraulic, and pneumatic).[11] Specifically, this research uses actuators made out of piezoceramics.

1.3 Piezoceramic Actuators

There are a number of different types of piezoceramic actuators being investigated for various applications. These include Moonie Actuators, Ring Type Actuators, RAINBOW actuators, THUNDER actuators and the LIPCA actuator.

1.3.1 Moonie Actuators

The Moonie actuator was developed by the material research group at Penn State in the early 90's by Xu.[11-12] The name "Moonie" comes from the moon shaped spaces between the metal end caps and the piezoceramic material.[13] Figure 1.2 shows that the Moonie consists of a piezoceramic disk sandwiched between two specially designed end caps.

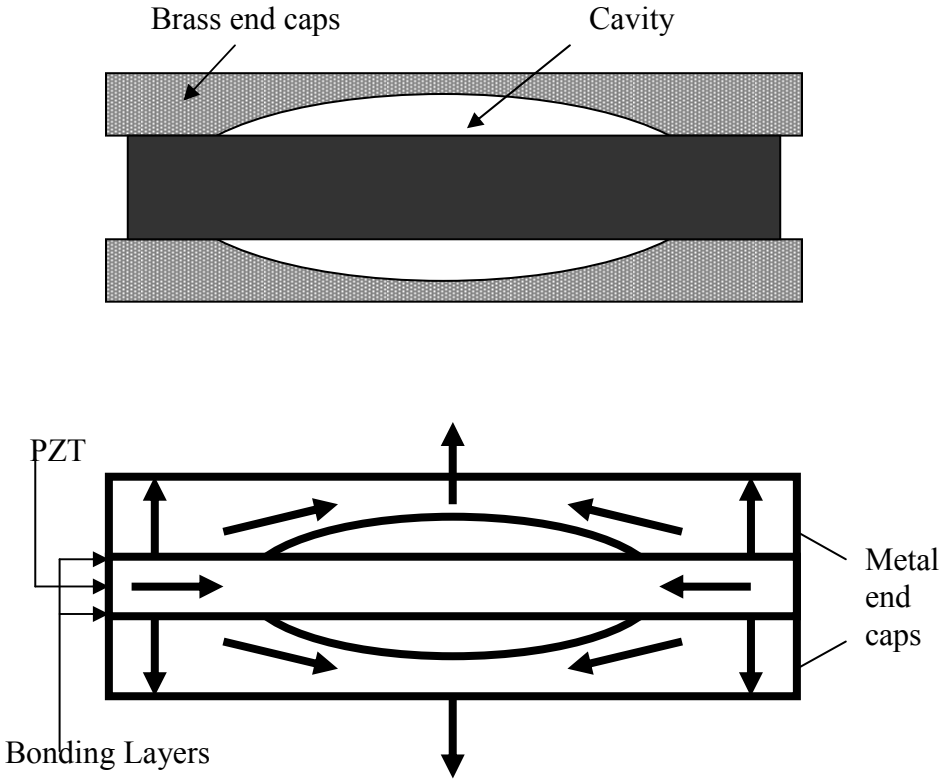

Figure 1.2 Moonie actuator. Arrows describe the direction of displacement.[12-13]

The end caps serve as mechanical transformers. They convert the lateral motion of the piezo material into a large axial displacement normal to the end caps. This configuration utilizes both the d_{31} and d_{33} coefficients of the piezoceramic.

Displacements for the Moonie Actuators at 1 kV range from 5 um with a resonant frequency of 80 kHz up to 23 um with a resonant frequency of 20 kHz.[12]

1.3.2 Ring Type Actuators

A close cousin to the Moonie Actuator is the ring type actuator. This actuator can be either a unimorph or bimorph configuration as shown in Figure 1.3.

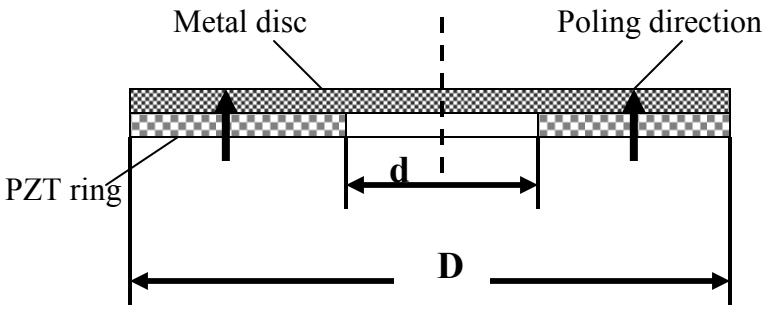

a) Ring type unimorph

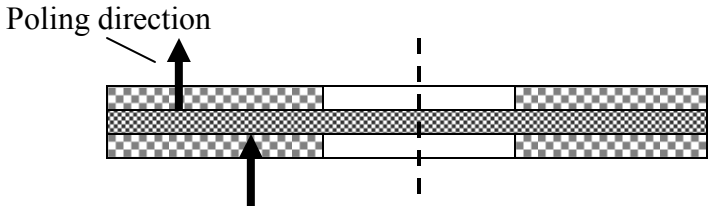

b) Ring type bimorph

Figure 1.3 Ring type actuators. a) Ring type unimorph. b) Ring type bimorph.[14]

With this actuator the ring-shaped piezoceramic radially contracts or expands and results in a large flexural displacement at the center of the metal disk. Much like the Moonie actuator, the displacement is largely dependant on the thickness of the metal and the stiffness of the actuator itself. Dong[14] built and tested these actuators at a variety of metal thickness and excitation voltages. He found that for a thin metal disk, the displacement of both the unimorph and bimorph were both around 90 um when excited at 400 V_{pp}.

1.3.3 RAINBOW Actuators

RAINBOW (**R**educed **a**nd **In**ternally **B**iased **O**xide **W**afer) actuators are stress-biased piezoelectric devices that produced much greater displacement than that of their counterparts (i.e. Moonies and Ring-Types). RAINBOWs are produced by chemically reducing one side of a lead-containing piezoceramic. The carbon used in the reduction process reduces the oxides of the PZT and produces a metallic lead layer on the disc. When it cools the difference in thermal expansion coefficients produces a stress-biased, domelike structure.[15-16] A schematic of a RAINBOW actuator is shown in Figure 1.4.

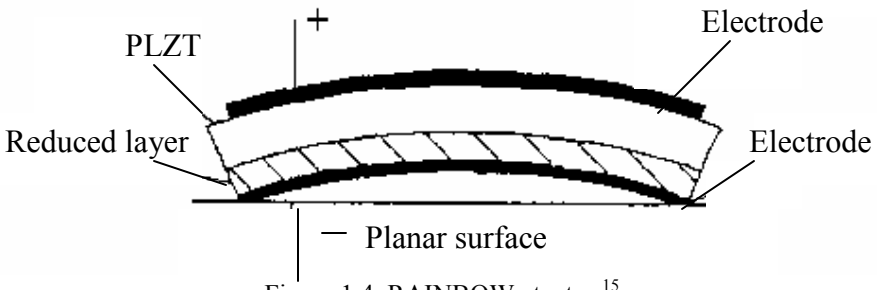

Figure 1.4 RAINBOW atuator.[15]

You can see from Figure 1.4 that the reduced side of the actuator is in compression while the top side is in a state of tension. Depending on the magnitude of stress and the thickness to diameter ratio of the piezoelectric wafer, the RAINBOW will have either a dome shape (as seen in the Figure) or a saddle shape. Once actuated in the d_{31} mode, the RAINBOW can displace by about 65 um at 600 V under a 0.5N load.[17] Also, these actuators can be stacked in series or parallel to increase the displacement even more.

1.3.4 THUNDER Actuators

The THUNDER™ (**Th**in **Un**imorph **D**riv**er**) was developed by NASA in the mid 90's. They are built by bonding thin piezoceramics to metal sheets by using a specially developed polymer adhesive.[16,18] The THUNDER™ actuator is a lot like the RAINBOW actuator in that is a stress biased actuator. The internal stresses induced in each THUNDER are due to the differences in the thermal expansion of the ceramic and the metal. When the actuator is processed it is heated and cooled and the aforementioned mismatch in thermal expansion coefficients causes the actuator to take on a dome like shape, much like the RAINBOW.[16] Figure 1.5 shows the lay-up of a typical THUNDER™ actuator.

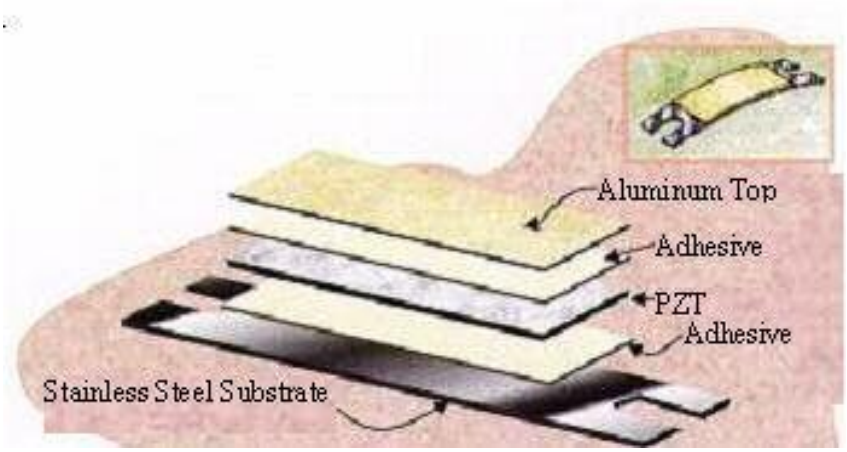

Figure 1.5 THUNDER™ actuator.[19]

Like the other actuators that have been discussed, there are a number of properties that effect the performance of the THUNDER actuator. Parameters such as load, geometry, number and thickness of metal and ceramic layers, curing temperature, boundary conditions, frequency and voltage all effect the overall performance of the actuator and must be tailored to fit the application in which the actuator is being used. Mossie[20] tested the THUNDER with simply supported boundary conditions and no load (conditions similar to those used to describe the performance of the Moonie, Ring Type, and RAINBOW actuators). In these tests the THUNDER™ produced a displacement of about 100 um at 325 V_{pp}.

Because THUNDERs™ and RAINBOWs are so similar it is nice to compare the two under the same conditions. This was done by Wise.[16] She varied the PZT thickness, percent of metal, load and excitation voltage and tested both actuators for many different combinations. The direct comparison tests showed that the RAINBOW actuators slightly outperform the THUNDERs ™. For example, at 500 V with 25%

metal and a PZT thickness of 0.508 mm the RAINBOW produced 175 um while the THUNDER™ produced slightly less displacement at 150 um. Similar differences were reported with changing load, voltage and percent metal.

1.3.5 LIPCA Actuators

The LIPCA (**Li**ghtweight **P**iezo-composite **C**urved **A**ctuator) is the final piezoceramic actuator that will be discussed. LIPCA actuators are being developed at Konkuk University in Korea. The are very similar to THUNDER™ actuators. The major difference is that LICPA adheres the PZT to composite lay-ups instead of metals. LIPCA uses the THUNDER™ like curved shape but because it is made with composites, with the bonding material contained in the composite, it is lighter and easier to manufacture.[21] Figure 1.6 shows what a typical LIPCA looks like.

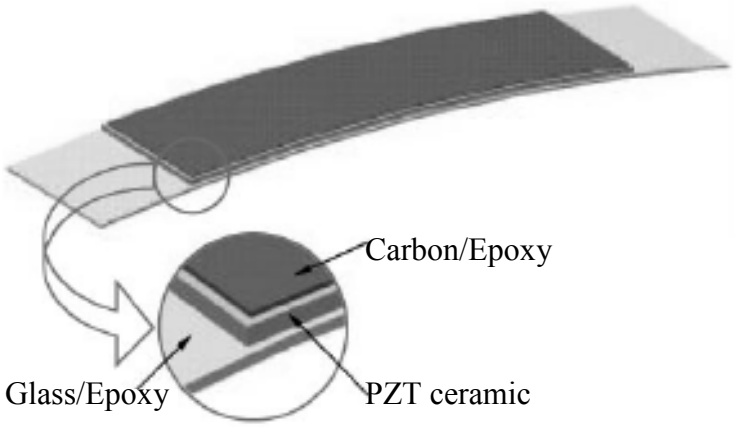

Figure 1.6 LIPCA-C1 actuator.[21]

Kim[22] designed, manufactured and tested five different LICPA actuators in order to determine what composite/ceramic lay-up yielded the best results. Based on his studies he was able to determine that to get the largest possible displacement it is desirable that the neutral axis be as far away from the piezoceramic layer as possible and that the bending stiffness be as small as possible. For the best design out of the 5 tested , LICPA-C2, a maximum displacement of 1.15 mm at 400 V_{pp} was achieved.

Kim also did a direct comparison of the LIPCA and THUNDER™ actuators[21] using the LIPCA design that most resembles the THUNDER™ (see Figure 1.5). The results of this test showed that at 400 V_{pp} LIPCA-C1 was able to attain a maximum displacement of 340 um while the THUNDER™ peaked at 190 um. In addition, LIPCA weighed 4.1 g while THUNDER weighted in at 7.3 g. This study shows that LIPCA has the potential to be a good alternative to the conventional metal-based piezoceramic actuators.

1.4 Recurves for Motion Amplification and Synthetic Jets

As stated in the previous section, actuators such as Moonies, RAINBOWs, etc. can be stacked in series or parallel in order to amplify their output displacement. One issue with these types motion amplifiers is that they are often built as external amplification schemes. The external packages have a tendency to be bulky and reduce the systems efficency.[23] Brei[23] proposed a recurve actuator that is a strain-amplifying building block that is used to increase direct material strains. The recurve configuration offers

actuators that are highly packable with high-energy-density. Figure 1.7 shows a schematic of a 6x2 recurve array.

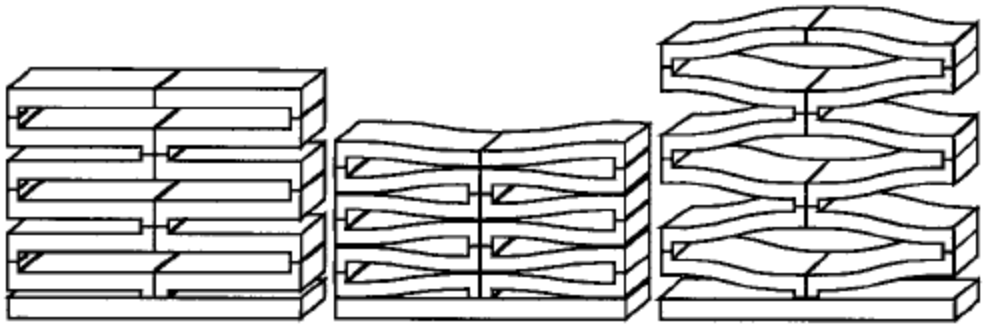

Figure 1.8 Recurve array (a) unactivated state
(b) activated state "pull" motion (c) activated state "push" motion.[23]

The idea behind the recurve is that it consists of two active piezoelectric sections. When one section is excited with a positive voltage and the other is excited with a negative voltage bending moments are created. These moments result in a positive moment for one section and a negative moment on the other section which in turn, results in a net transverse tip displacement *w*. In the case of a cantilever beam, the advantage of a recurve is that the ends deflect without any rotation.[24] This recurve effect, in both the undeformed and excited state, is shown in Figure 1.8. In this figure *w* represents the displacement of the beam.

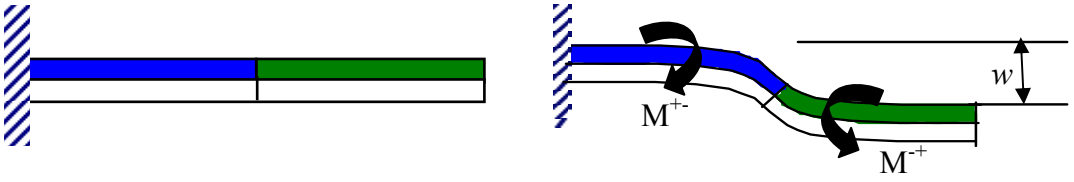

(a) undeforemed (b) under excitation

Figure 1.8 Typical recurve element (a) undeformed (b) under excitation.[24]

Recurve benders have been shown to provide an efficient piston type motion to drive synthetic jets for active control.[25] The recurve configuration acts as a motion amplifier that can change a low displacement, high force actuator into a high displacement, low force actuator.[25] The higher displacement of the vibrating membrane allows more momentum in and out of the synthetic jet orifice which increases the momentum of the jet ejected into the free stream. The segmented configuration allows for even more peak displacement while there is zero stain where the segments meet. To date these recurve synthetic jets have been built and tested using both PVDF film and PZT ceramics as the active material.

1.4.1 PVDF Benders

PVDF (Polyvinyldene Flouridene) is a material the exhibits the piezoelectric effect. It's high energy density make it a good option for synthetic jets (d_{31} = 23e-12 m/V). In addition, it is easy to manufacture as a thin film at low cost and it is readily

available. Because the film is thin and lightweight when compared to other synthetic jet components (piston, housing, etc) it can be easily stacked to amplify motion without significantly increasing the synthetic jet mass.[24] Figure 1.9 shows what a stacked PVDF bender looks like in it's retracted and extended state. The Figure also shows what a typical lay-up of a multiplayer Kynar® PVDF film beam is comprised of.

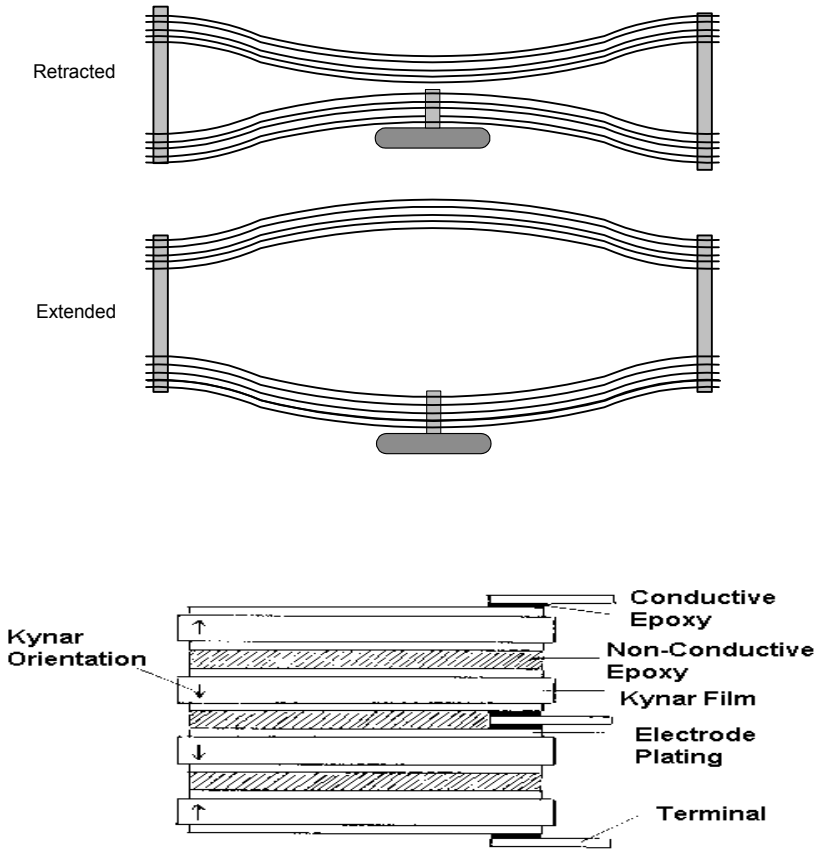

Figure 1.9 (a) PVDF bender in it retracted and extended state, (b) lay-up of PVDF beam.[24]

Results from Calkins and Mabe[24] showed that at 400 V_{pp} the PVDF bender synthetic jets can achieve a 5.5 mm displacement and a 23 m/s velocity out of the synthetic jet slot (orifice). While the other actuator (Moonies, Ring-Type, RAINBOWs, etc.) did not have velocity data available, the available data shows the displacements from the PVDF actuators are as much as 1.5 magnitudes larger.

1.4.2 Piezoceramic Bimorph Recurve Actuator

Although the PVDF based synthetic jets seems to perform well, Clingman has proposed using PZT ceramics to build the recurve. The design, building, and testing of these PZT bender synthetic jets is the focus of the research discussed in the remainder of this thesis.

The PZT recurve is essentially a bimorph version of the LIPCA-C1 that utilized the recurve technology. In order to achieve the recurve shape a thin strip of electrodes is etched off at the ¼ and ¾ lengths. The middle electrode segment is then actuated 180 degrees out of phase with the end segments. Figure 1.10 shows the PZT recurve confiuation and Figure 1.11 shows how two PZT recurve actuators can be used to create a synthetic jet. In addition, Figure 1.12 shows a dual actuator synthetic jet which will be discused later in this thesis.

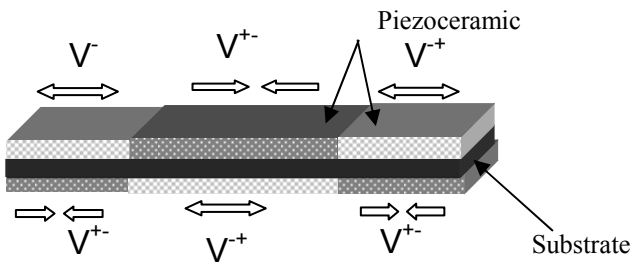

Figure 1.10 PZT recurve configuration.

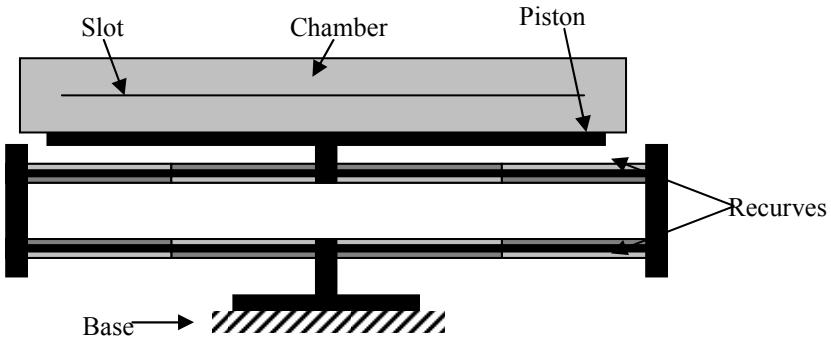

(a) undeformed

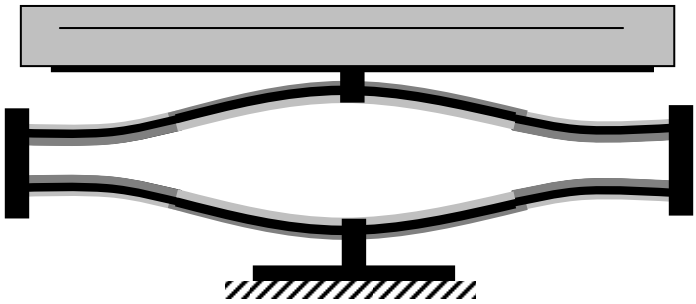

(b) under excitation

Figure 1.11 PZT recurves attached to a synthetic jet piston.

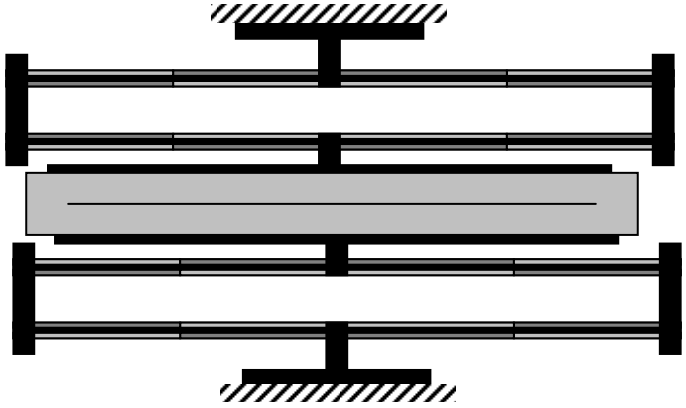

(a) undeformed

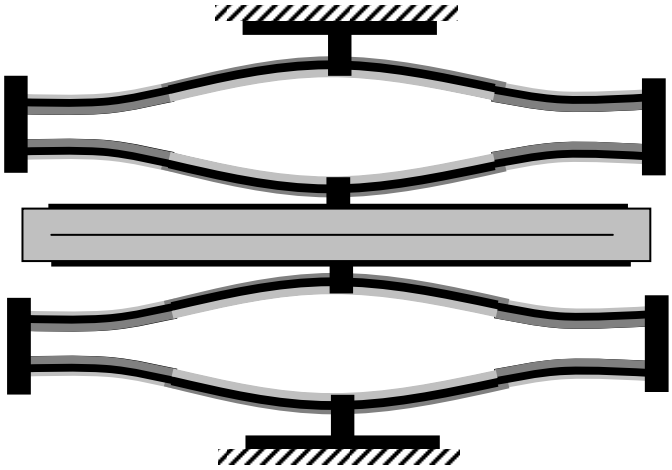

(b) under excitation

Figure 1.11 PZT dual actutator synthetic jet.

The next chapter will go into detail about the construction of the PZT recurve actuators and the subsequent chapters will discuss testing and modeling of the synthetic jets. The tests will show that the PZT recurve outperforms the other PZT actuators described above and is also comparable in performance to the PVDF bender.

Chapter 2: Actuator Design and Construction

2.1 Actuator Construction Process

The UMD actuator is built by sandwiching a piece of 8-mil (.2032 mm) carbon fiber prepreg between two 10-mil (.254 mm) piezos. The piezos used for most of the actuators was PZT-5A ordered from Piezo Systems, Inc. The piezo sheets come as a 7.24 cm x 7.24 cm square. Because of the size of the piezo sheet, the length of the actuator was limited to 7.24 cm. In order to give the 0.5" actuator a mid-range aspect ratio a width of 1.27 cm was chosen. Thus, the first step it to cut the piezo to the desired size, 1.27 cm x 7.24 cm. This is a simple process. It involves simply using a straight edge and a sharp knife. Because PZT is very fragile and tends to crack easily, much care must be taken when cutting. Figure 2.1 shows how the PZT is cut.

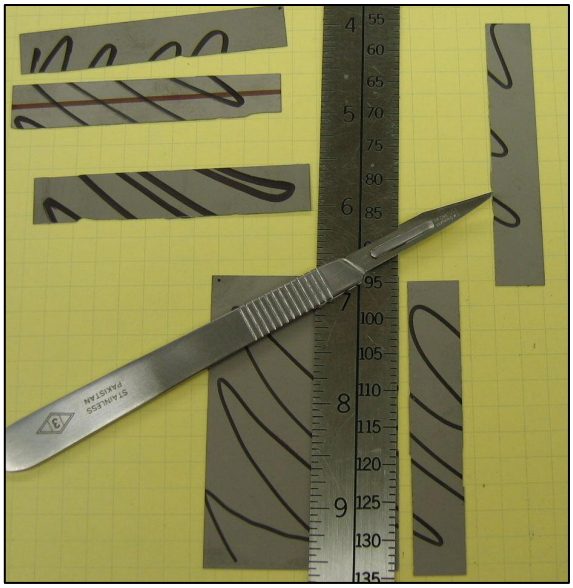

Figure 2.1 Cutting of PZT.

Once the PZT is cut to the correct sizes the carbon pre-preg is sandwiched in between the two piezos. The carbon used was the unidirectional carbon epoxy prepreg DA 911U. Also, small amounts of conductive epoxy were placed between the carbon and the PZT. This was to ensure that when the carbon was grounded the back side of the PZT would also be grounded. The actuators were then taped to a metal plate and cured at 400^{o}F for 1 hour. Figure 2.2a is a photo that shows how the actuators are prepared before curing.

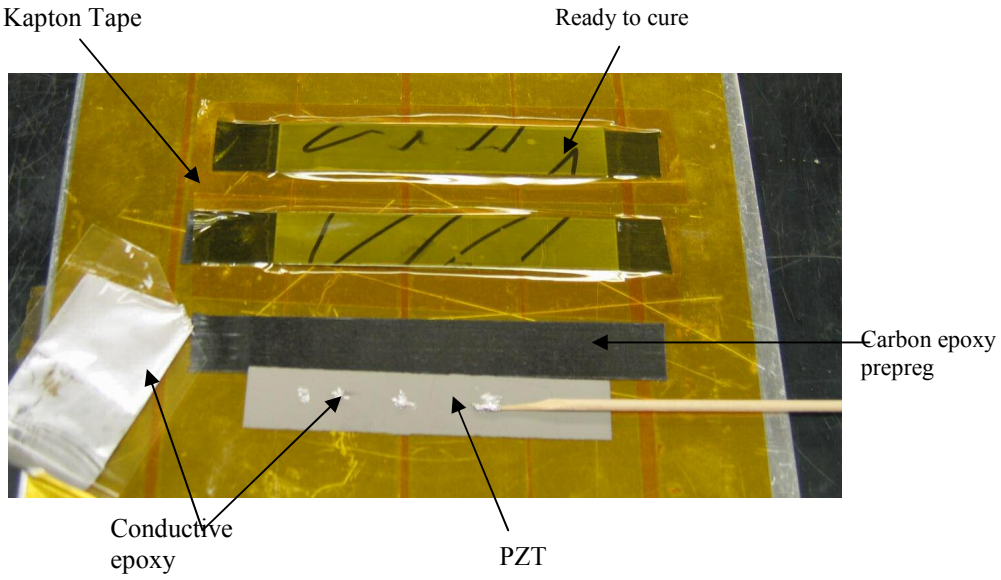

Figure 2.2a Preparation of actuators for curing.

Once the curing process is complete a thin strip of fiberglass fibers combined with conductive epoxy is placed along the length of the piezo. This provides added strength and helps keep the piezos from cracking when they are actuated. This process is shown in Figure 2.2b.

The conductive epoxy used in the fiberglass strips was the same as that was used to ground the back side of the PZT. It is called Cho-Bond 584-29 and is from Chromerics, Inc.

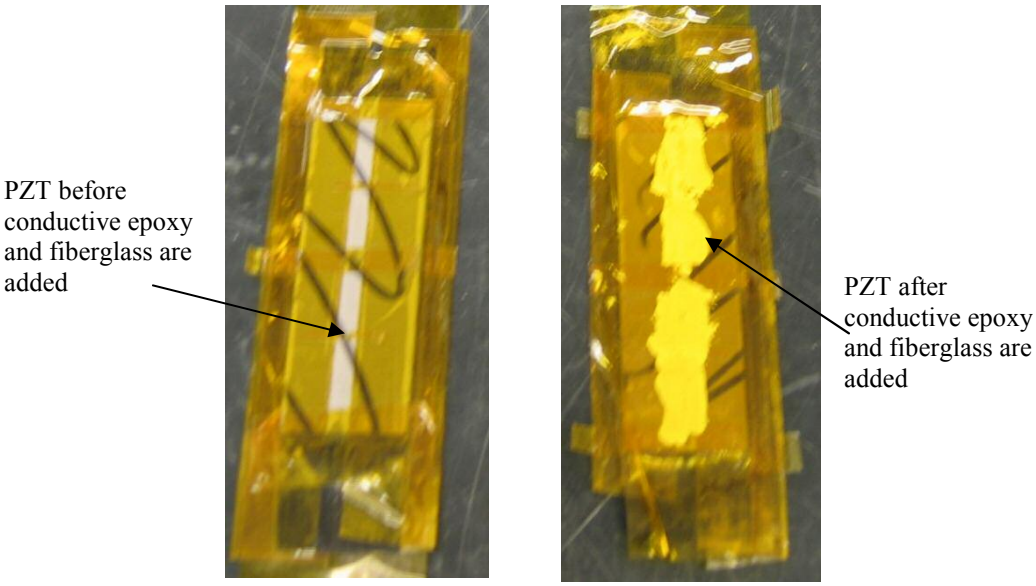

Figure 2.2b Preparation of actuators for curing.

Once the carbon prepreg is cured for 15 minutes at 235°F a thin strip of electrodes is etched off at the ¼ and ¾ lengths. This allows for the recurve configuration. Finally, all the positive segments are wired together and all of the negative sections are wired together. To ensure that shorts don't occur where the wires pass over the top of the PZT, a small amount of 5 minute insulating epoxy was placed on the top so that there could be no contact between the wires and the top of the PZT. A close up of the etching, the epoxy boundary, and the wiring can be seen in Figure 2.3.

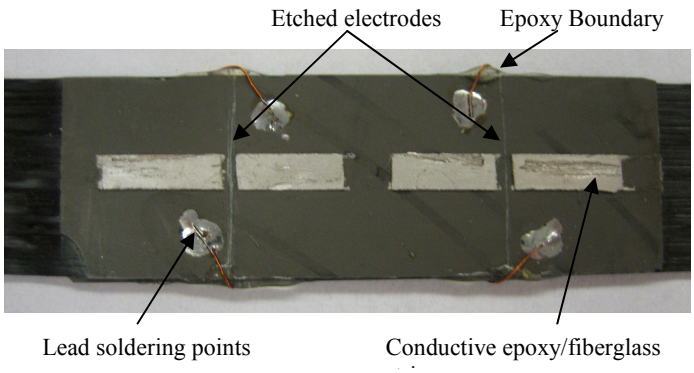

Figure 2.3 Etching and wiring of actuator.

Once the actuators are wired, two of them are connected together to form the recurve for the synthetic jet. A lightweight G-10 fiberglass was used to hold the two piezo recurves together and provide a clamped boundary condition at the ends. The G-10 and the piezos were secured together with 5 minute epoxy. G-10 is also used to connect the piston and the base to the middle of the recurves. This is seen in Figure 2.4.

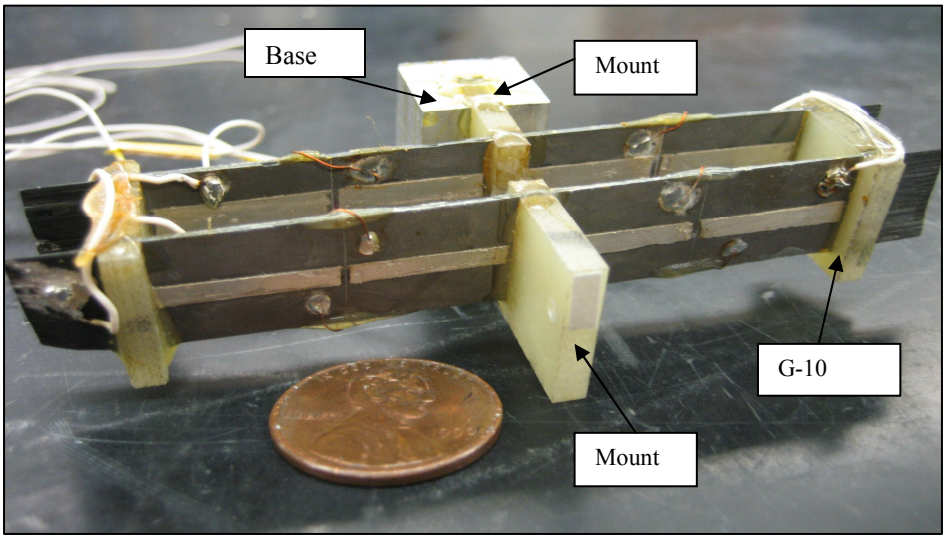

Figure 2.4 Actuators mounted into recurve configuration.

Once the actuators are built they are connected to a piston which is connected to a chamber via a flexible membrane. The sizes of both the piston and chamber varied depending on the application. This will be discussed further in the next section. The piston and the chamber are connected by using double sided tape on the chamber surface and latex to form a flexible membrane for the walls of the chamber. This is shown in Figure 2.5.

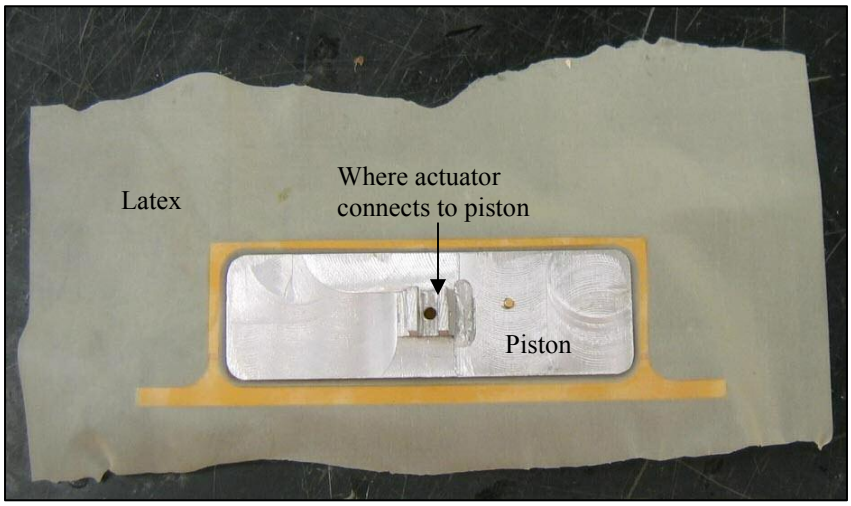

Figure 2.5 Chamber construction.

Once both the chamber and the actuator are complete, they are put together to form the synthetic jet.

Initially, two synthetic jets were built using two different piezo materials, PZT-5A (d_{31} = -185e-12 m/V) and PLZT-98 (d_{31} = -400e-12 m/V). The difference in these two piezoceramics is the d_{31} piezoelectric coefficient. The coefficient d_{31} is the

amount of strain in the 1-direction due to an applied electric field in the 3-direction. For these actuators the 1-direction is along the actuator length and the 3-direction is perpendicular to the actuator length (along the thickness). The PLZT-98 has a d_{31} twice that of the PZT-5A so for the same applied voltage, the PLZT-98 will produce twice the strain. Using both types of piezos a single actuator synthetic jet and a dual actuator synthetic jet were built. Figure 2.6 shows a fully constructed single actuator synthetic jet made using the PZT-5A and Figure 2.7 shows the dual actuator synthetic jet made using the PLZT-98.

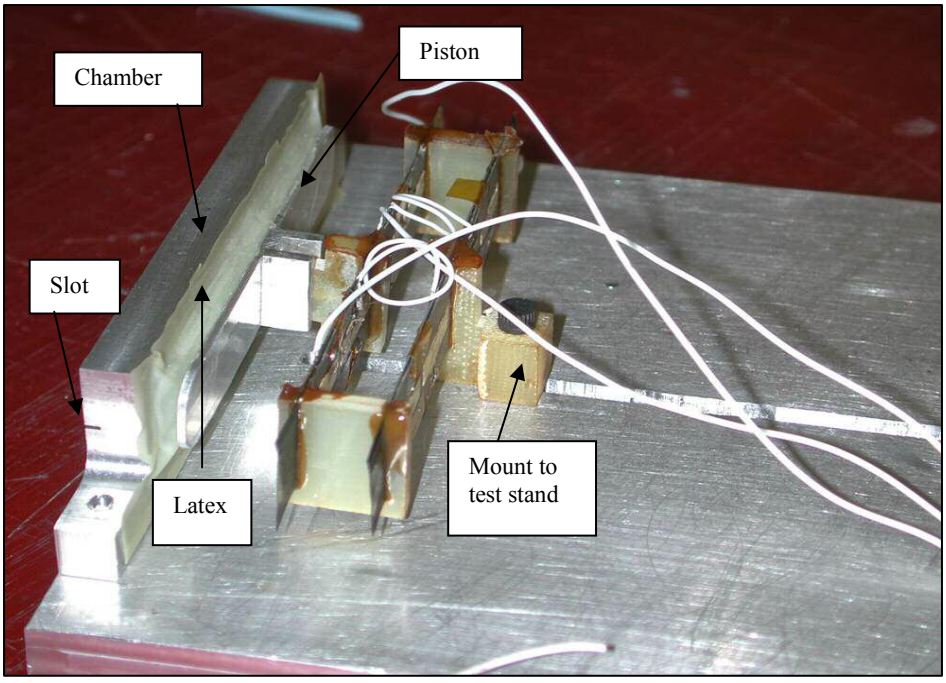

Figure 2.6 Single actuator synthetic jet.

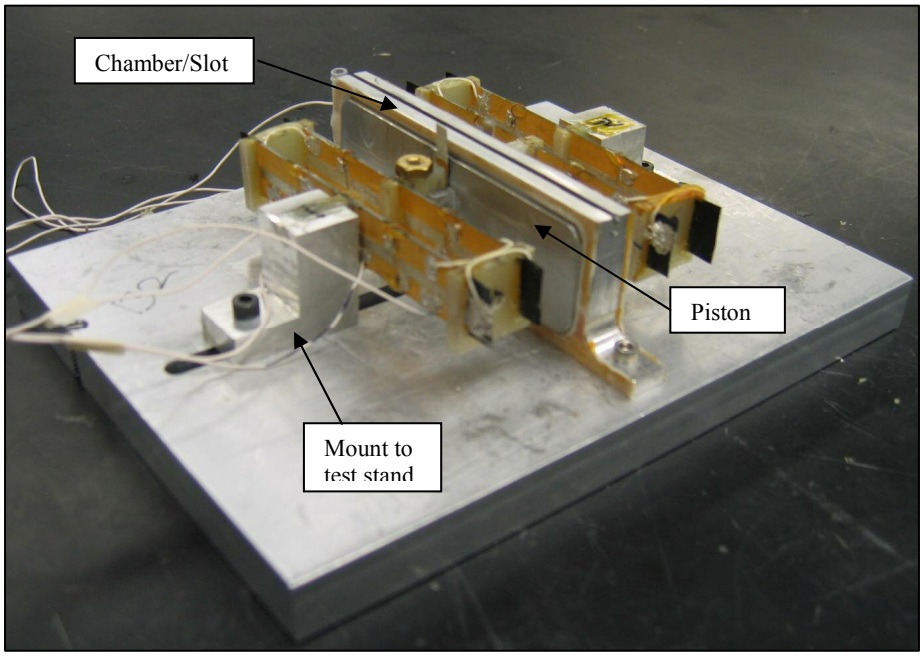

Figure 2.7 Dual actuator synthetic jet.

The chamber and slot sizes of the single and dual actuators differ slightly. This is because once data was collected from the single synthetic jet modifications were made to the dual actuator size to maximize it's performance. Table 1 shows the dimensions and mass of both actuators.

Dimension	Single Actuator	Double Actuator
slot length (mm)	73.66	73.66
slot width (mm)	0.508	1.143
piston width (mm)	1.016	22.86
piston length (mm)	73.66	73.66
chamber volume (cm^3)	6.55	14.75
mass (g)	17.9	49.6

Table 1. Synthetic jet dimensions.

Once the actuators were built, displacement, velocity, pressure and block force data was collected. The sensors used to collect this data as well as the calibration processes are discussed in the appendix.

Chapter 3: Synthetic Jet Performance

3.1 Single Actuator Synthetic Jet

3.1.1 Displacement and Velocity Output Results

Synthetic jet air velocity and piston displacement data were collected using the pressure sensor and the laser displacement sensor discussed in Appendix 2. Initial tests of the single actuator made using Rockwell Scientific PLZT-98 high energy density piezos produced +/- 1.143 mm (+/- 45 mil) piston displacement and 25 m/s air flow velocity out of the chamber. These tests were run at 200 volts peak to peak and 125 Hz, the resonant frequency of the system. The displacements and velocities measured using the PLZT-98 were approximately twice that of subsequent tests conducted using the recurve actuators built using standard PZT-5A. This is the expected result. Because the PLZT-98 has twice the energy density of PZT-5A it should produces twice as much displacement and velocity output per unit input power. Figures 3.1, 3.2 and 3.3 show the displacement and velocity output of each actuator.

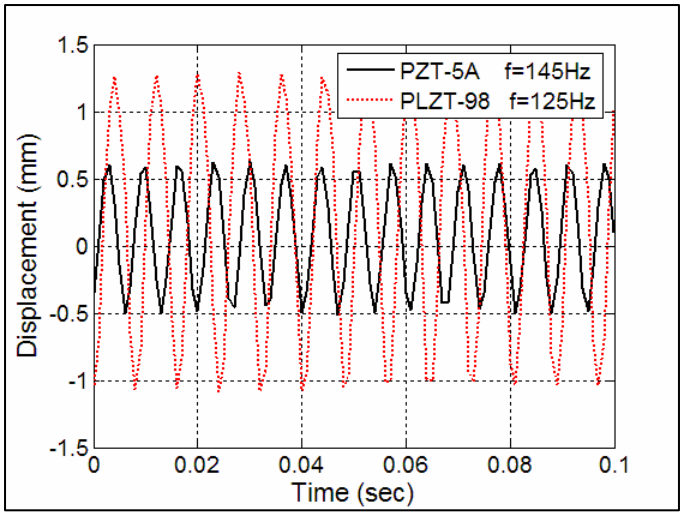

Figure 3.1 Displacement of single actuator synthetic jets at 200 V_{pp}.

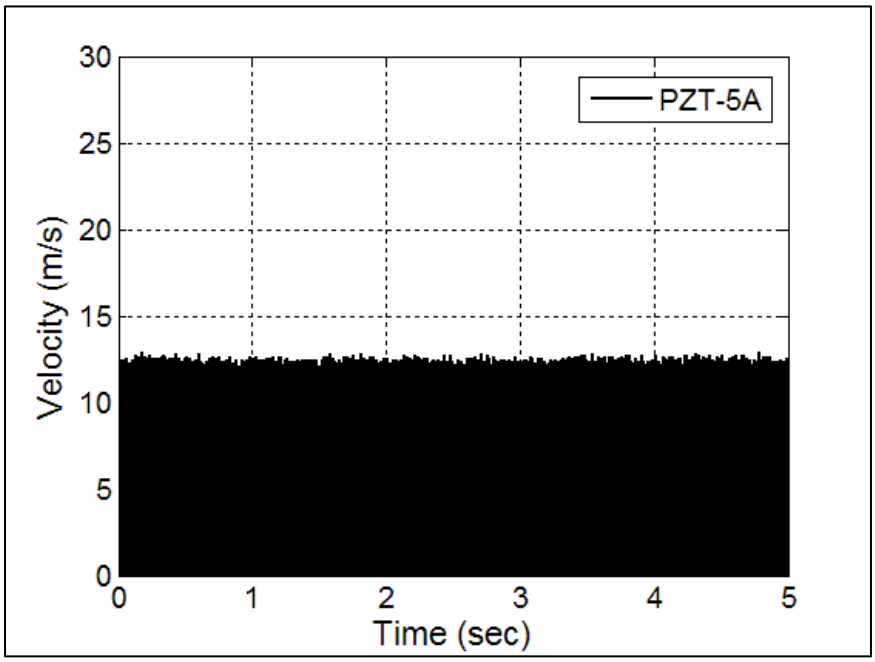

Figure 3.2 Velocity output of PZT-5A synthetic jet at 200 V_{pp} and 145 Hz.

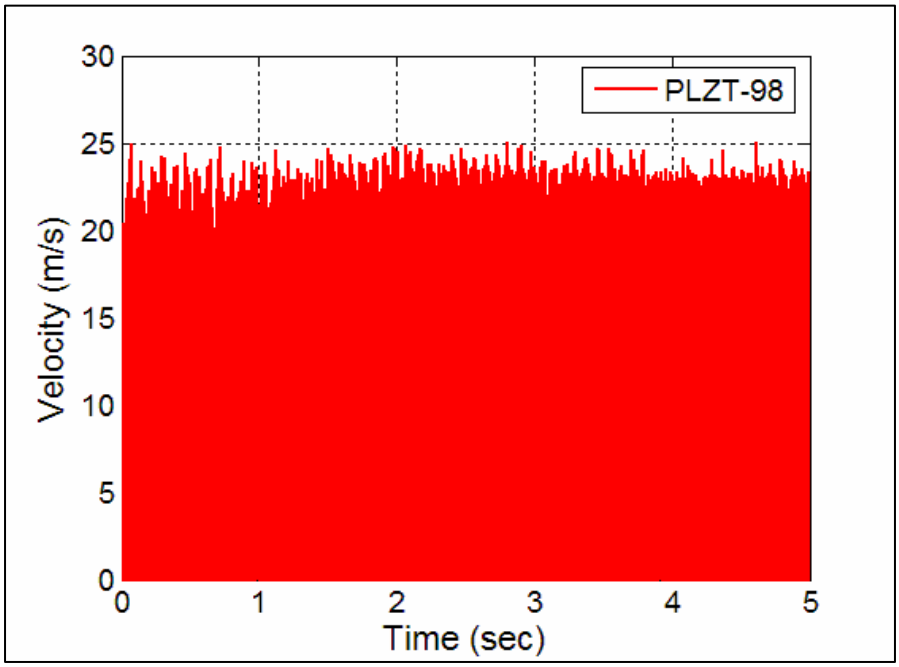

Figure 3.3 Velocity output of PLZT-98 synthetic jet at 200 V_{pp} and 125 Hz.

3.1.2 Endurance Test Results

In addition to velocity and displacement tests, endurance tests were run to determine when and if the actuator would fail. A single bimorph synthetic jet was powered up and left to run. The goal of this test was to reach a billion cycles before failure. This goal was met after two months of continuous actuation at frequencies ranging from 100 to 160 Hz. One result that the endurance tests showed is that the natural frequency of the synthetic jet decreases with time. Figure 3.4 shows this.

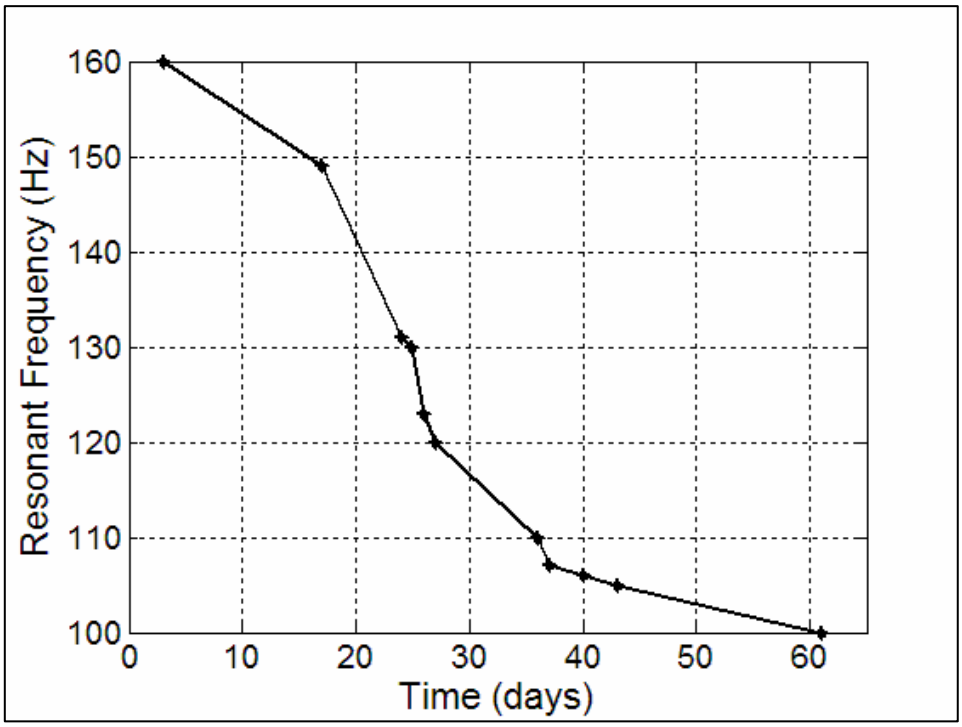

Figure 3.4 Resonant frequency during endurance tests.

We see that initially the resonant frequency was 160 Hz and after 61 days it has drifted to 100 Hz. This frequency drift could be due to a number of different things. It is possible that as the actuator cycles there is a reduction in stiffness of the actuators because of loosening of the bonds between the carbon and the piezos. It could also be

caused by microscopic cracks in the piezo. Lastly, it is possible that the frequency drift is due to the change in resistance of the latex and had nothing to do with actual piezo structure itself. Future work includes looking at the actuators under a microscope and re-running the test without the actuator connected to the chamber to see if the reason for the degradation can be determined. As stated above, the goal of this test was to make it to a billion cycles. Thus, once this goal was met the tests were terminated. Unfortunately, one question that is left unanswered is whether the resonant frequency would have continued to drop until a complete failure of the system occurs or the resonant frequency would have eventually stabilized.

The endurance test also involved looking at the changes in displacement over time. Figure 3.5 shows this data broken up into four sections.

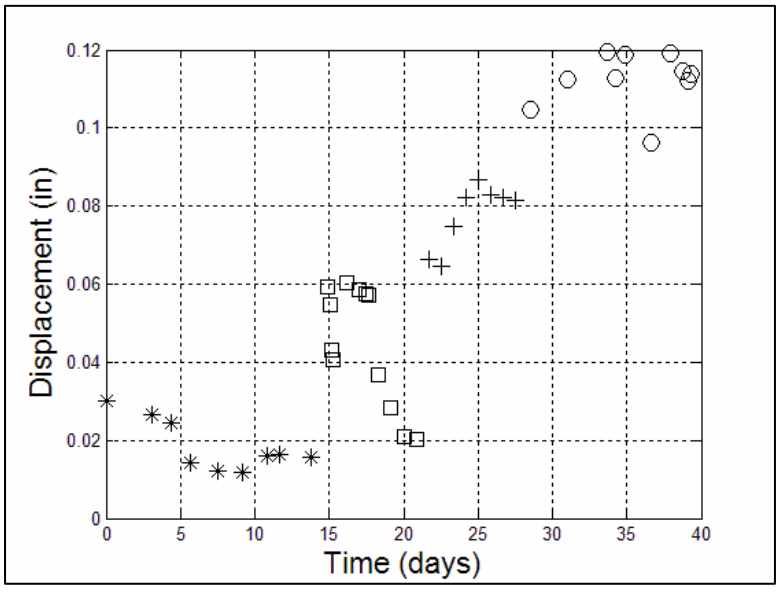

Figure 3.5 Displacement during endurance tests.

The first section of data shows the initial data collected during days 1 through 15. The actuator was running at 75 volts and 160 Hz and was initially getting 30 mils peak to peak displacement. We see that as time goes on the displacement begins to fall. There are two reasons for this. First, as time goes on the resonant frequency drifts (as seen in Figure 3.4). Because the excitation frequency was initially set and left at 160 Hz, as the resonant frequency drifted the synthetic jet was no longer running at it natural frequency. This caused the performance to degrade. Second, during the initial portion of the tests we experienced some problems with the leads coming off. Obviously this degraded the performance as well. At day 11 there is an increase in the displacement, this is a result of fixing the leads. On about day 15 the second phase of testing commenced and the excitation voltage was increased to 150 volts and a frequency of 150 Hz. Again, during this portion of the test there were frequency drift and broken lead problems. The dramatic dip at the beginning of the "□ data" is a result of a broken lead and the gradual decline at the end of this section is due to frequency drift. Next we look at the third section of the data. Unlike the first two sections of data, the "+ data" increases as time goes on. On day 22 the excitation frequency was adjusted to 132 Hz, to match the current natural frequency of the system. This caused the displacement to jump to 60 mils. This is twice the day one displacement which is expected for twice the excitation voltage. However, for this section data we see that although the excitation voltage remained constant the displacement increases. There are two possible reasons for this. One is that we were adjusting the frequency daily to ensure the system was always running close to it's natural frequency. This alone would most likely avoid a decrease in displacement

amplitude and would not explain an increase in displacement. The second and more likely source of the observed increase is that at this point in time the latex is becoming fatigued and is starting to tear more and more each day. This dramatically decreases the damping of the system. The fourth portion of the data starts at about day 30 when the remaining latex was cut away and the bimorph was left to run without any interaction with the chamber. This "○ data" shows that the free displacement of the bimorph (with damping close to zero) is around 120 mil peak to peak. This operation was with the 150 V_{pp} excitation and a frequency that ranged from the 115 Hz down to 100 Hz as show in Figure 3.4.

3.2 Dual Actuator Synthetic Jet

3.2.1 Velocity Output Results

As with the single actuator synthetic jet, velocity data for the dual actuator was taken with a pressure sensor. Figures 3.6 and 3.7 show velocity data from both the PZT-5A and PLZT-98 actuator respectively. We see that both plots have a maximum velocity output around 23 m/s; this is because the PZT-5A actuator data was excited at 200 V_{pp} while the PLZT-98 actuator was excited at only 100 V_{pp}. Previous tests had shown that when the PLZT-98 was run at the higher voltage the strain on the piezos caused them to crack at their highest stress points. This is important because it has allowed us to determine that although the PLZT-98 has a much higher energy density that PZT-5A, in recurve actuator applications it is difficult to harness the energy without damaging the piezo. In addition, the PLZT-98 is much more expensive then PZT-5A. For these two reasons, the 5A is most likely better option for this application.

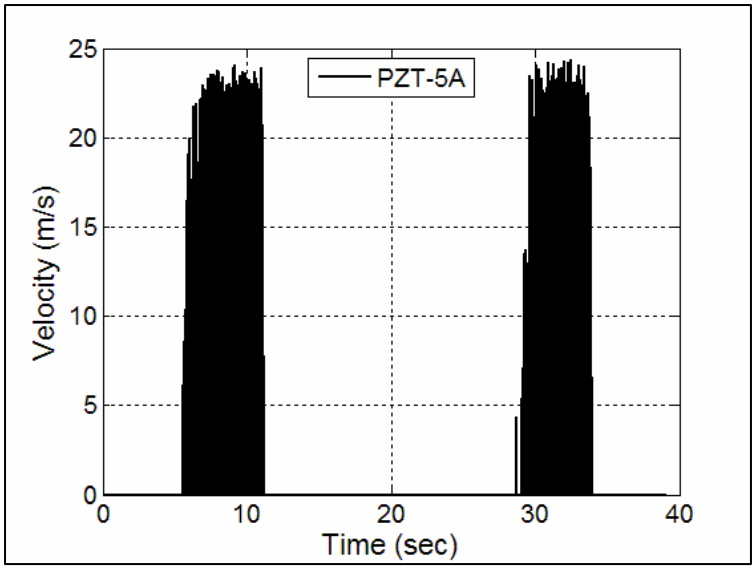

Figure 3.6 Velocity output of PZT-5A dual synthetic jet.

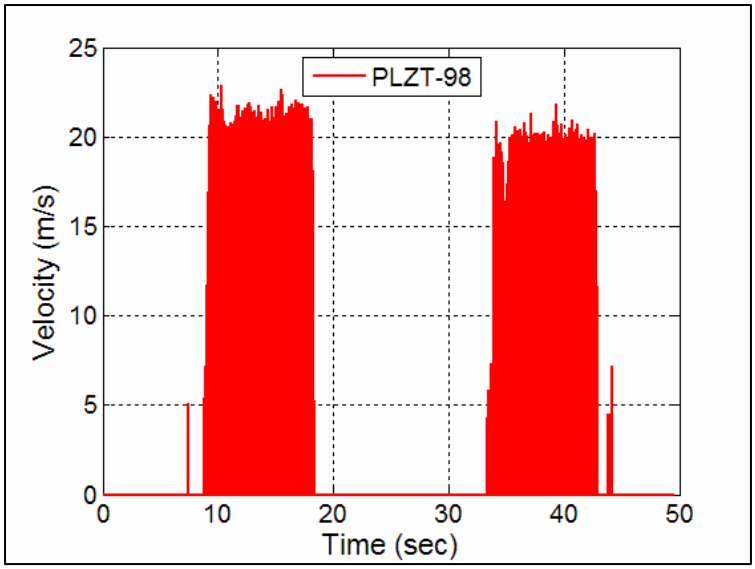

Figure 3.7 Velocity output of PLZT-98 dual synthetic jet.

The data in Figures 3.6 and 3.7 was obtained by passing a pressure sensor back and forth across the chamber slot. The peaks in the data represent points in time when the pressure sensor was held directly over the slot where as the velocities near zero m/s are points in time when the pressure sensor was not over the slot. Figure 3.8 shows a picture of how the pressure sensor is held over the slot when it is reading the higher velocities.

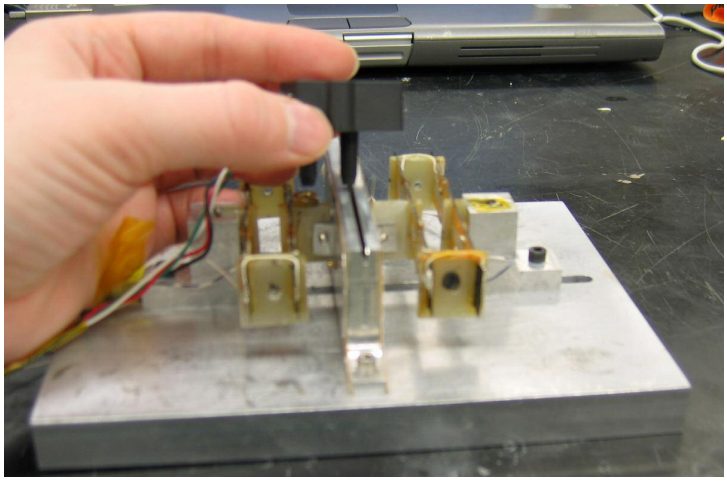

Figure 3.8 Taking velocity data of synthetic jet.

3.2.2 Phase Matching of Dual Actuator

The increased velocity output produced from the dual actuator is desirable; however, this configuration presents the challenge of making sure both actuators have the same resonant frequency and phase. Since no two actuators are exactly the same, chances are they will not have the same resonant frequency using a single excitation signal. This presents a problem when trying to run two synthetic jets at resonance. Thus, small masses were added to the actuators until their resonant frequency matched. In addition, we wanted to determine how sensitive the velocity output was to the phase offset between the two actuators. The initial thought was even a small mismatch in phase between the two actuators could cause a significant loss in velocity output. With the actuators out of phase, during the portion of each cycle when one side of the synthetic jet was pushing air out, the other side would be working against it by sucking the air back in. That was not the case. For this test one of the actuators was used as a reference and the phase of the second actuator was varied to introduce a phase lag from 0 to 180 degrees with respect to the input to the reference actuator. Figure 3.9 shows the results of this test.

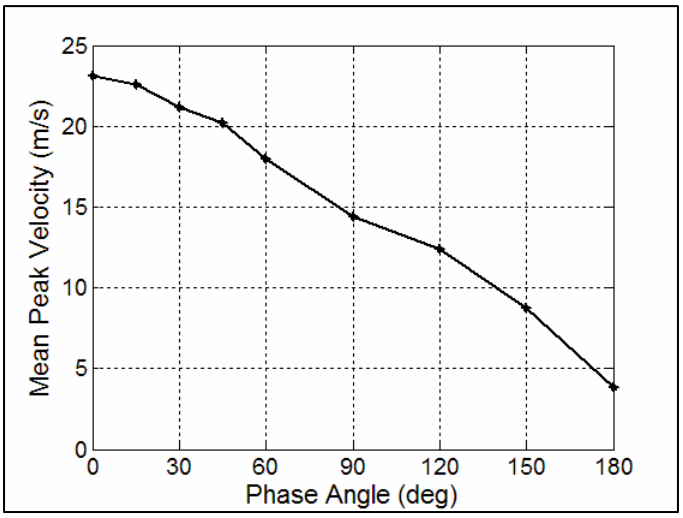

Figure 3.9 Peak Velocity for dual synthetic jet at varying phase angles

This data shows that phase angle differences of up to 15 degrees resulted in a decline in velocity output of less than 2.2 percent. Even a phase offset of up to 30 degrees only reduces the velocity output by 8.5 percent. This proved we didn't have to worry about small phase differences between the two actuators.

Chapter 4: Actuator Design Comparisons

4.1 Results of Varying Chamber Slot Size

As mentioned in the introduction, the size of the air slot in the chamber can have a dramatic effect on the performance of the synthetic jet. For a given synthetic jet with a constant blocked force and chamber volume one would expect that a smaller slot would allow more pressure to build inside the chamber. This build up of pressure will effect both the displacement and the velocity output. A higher pressure in the chamber will result in a larger force pushing the air out of the slot (increase in velocity) and a larger force pushing against the piston motion (decrease in displacement).

In order to validate this theory, chamber pressure, displacement and velocity output data were collected for the synthetic jet at varying slot lengths. The width of the slot was constant at 1.143 mm and the slot length was varied from 1.27 mm to 73.66 mm (0.05" to 2.9"). Since the chamber pressure and the jet velocity are measured using the same sensor, two sets of data were taken for each slot size. The first set contained information on the chamber pressure and piston displacement while the second set (taken immediately after the first) contained information on the jet velocity. All of the data was collect at 200 V_{pp} and at the resonant frequency of 156 Hz.

Figure 4.1 shows a plot of slot length versus chamber pressure. One can see that the pressure does in fact increase with decreasing slot length. The original data set is

represented in the plot by the black stars. Looking at this data set we see that the majority of the points fall on a fairly linear line. The two obvious exceptions are the two points at slot lengths of 6.35 mm and 11.43mm. In order to determine whether or not these points were outliers more data was collected at the smaller slot lengths. These points are shown as red circles. After plotting the additional points it appears the overall trend is more asymptotic than linear. The additional points that were taken seem to indicate that the pressure at a slot length of 1.27 mm is closer to 700 Pa and that the original point is an outlier.

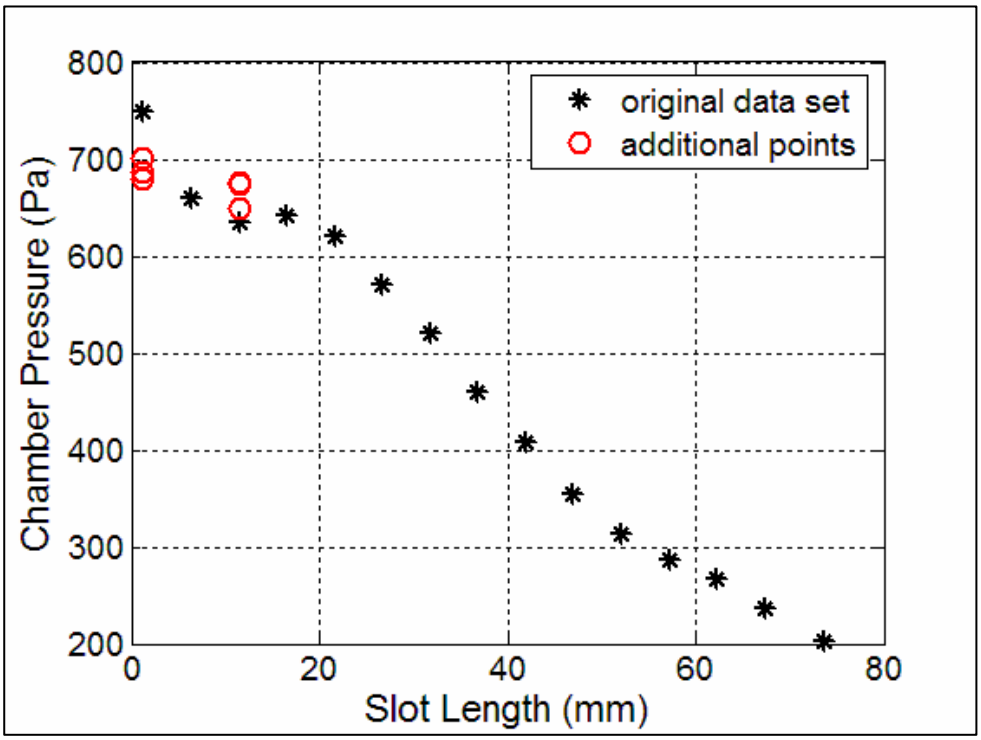

Figure 4.1 Chamber pressure at varying slot lengths.

Figure 4.2 shows the displacement data that was collect along with the pressure data. Again, the original data set is represented with the black stars and the additional data

points are shown as red circles. One can see that unlike the additional pressure points, the additional displacement points fall right in line with the original data set. This shows that the pressure displacement is much more consistent than the pressure reading. In addition, for the given synthetic jet set-up the displacement of the piston when attached to the latex membrane levels out around 1.1 mm.

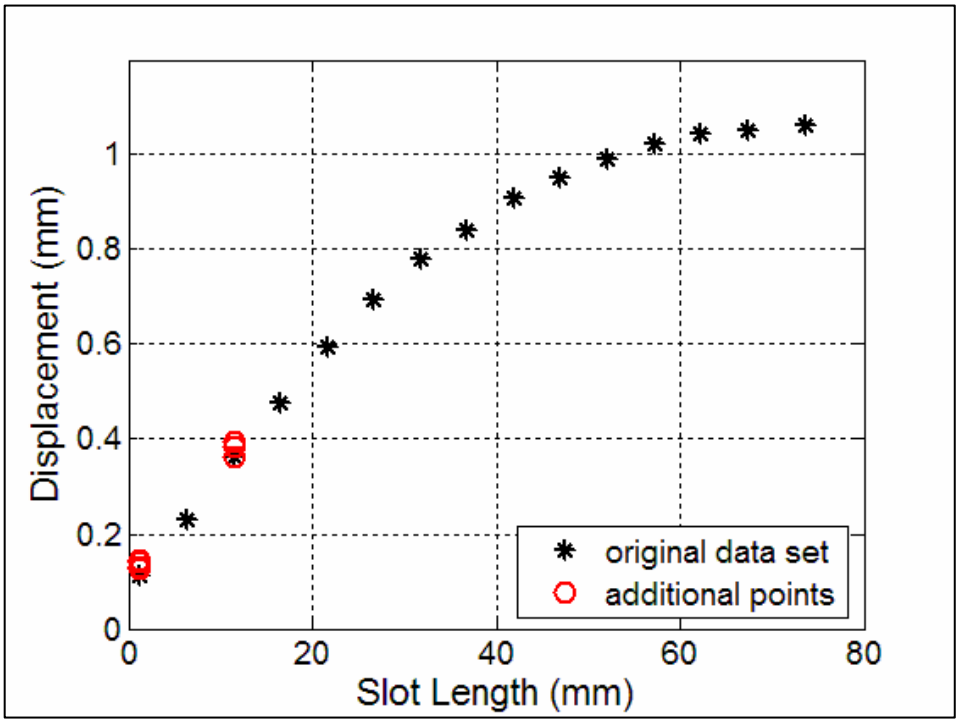

Figure 4.2 Piston displacement at varying slot lengths.

The velocity output measurements were taken immediately after the displacement and pressure readings. The slot length vs. velocity output is shown in Figure 4.3. The Figure shows that the maximum velocity is 30 m/s for a slot length of 1.27 mm. Unfortunately, depending on the application this slot size may be too small for use on

a large scale vehicle. For large air vehicles flow control that can span a larger area may be necessary. For this case the longer slot length would be desirable. In this case we see that the velocity output this actuator can produce is 13 m/s with a 73.66 mm slot.

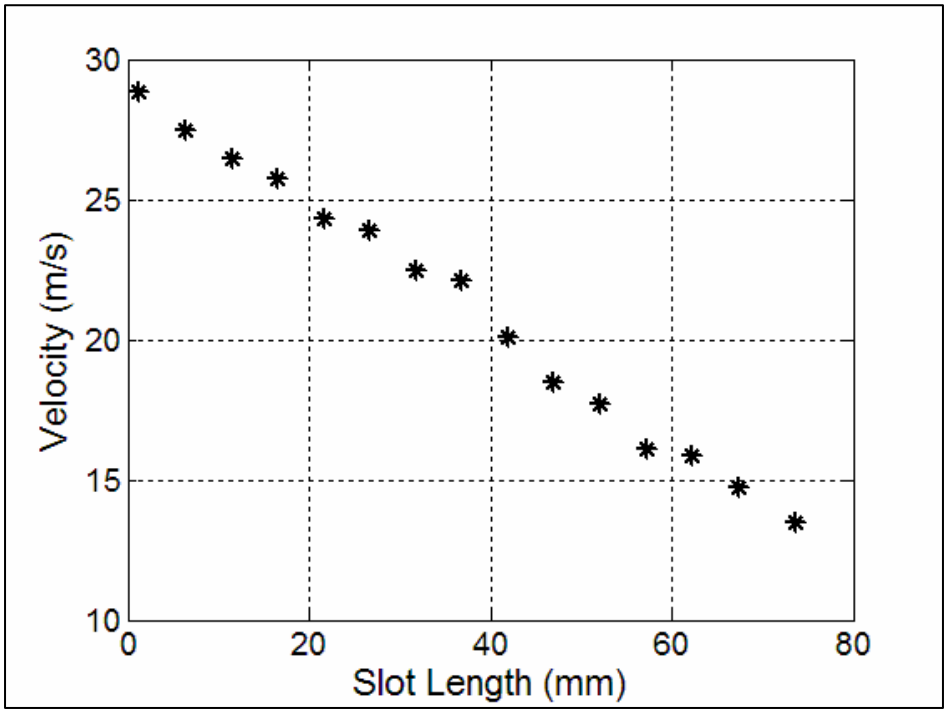

Figure 4.3 Jet velocity at varying slot lengths.

4.2 Results of Varying Actuator Dimensions

Another factor that can affect actuator performance is the geometry of the bimorph. Results from a synthetic jet model (to be discussed in Chapter 5) suggest that a bimorph that has less length and more width may supply a larger jet velocity. In order to test this, two bimorphs with the same area (same amount of active material)

but with different dimensions were tested and compared. The original bimorphs dimensions were 1.27 cm x 7.2 cm (0.5" x 2.85"). This was the dimensions of one of the actuators used for the comparison. The second actuator was added and it's dimensions were 1.778 cm x 5.17 cm (0.7" x 2.036"). Free displacement, resonant free displacement, blocked force, piston displacement, chamber pressure and jet velocity were measured for both actuators. The voltage was varied from zero to 200 $V_{pp.}$ For the free displacement and blocked force, the data was taken at the lowest frequency possible for the given set-up, 1 Hz. All the other data sets were taken at the actuator's natural frequency. For the 0.5" actuator the natural frequency was 124 Hz without the piston and 105 Hz when attached to the chamber and latex membrane. The 0.7" actuator had a natural frequency of 230 Hz without the piston and 213 Hz when connected to the chamber.

Figures 4.4 and 4.5 show the free displacement and resonant free displacement of the actuators. The free displacement is the displacement the actuator can achieve when it not hooked up to the piston and the chamber. This is the displacement without the effects of the extra mass of the piston and without the damping from the latex membrane.

One can see that in both cases the slope of the 0.5" actuator is greater than that of the 0.7" actuator. This is as expected. The longer, thinner actuator is less stiff thus allows for more displacement. At 170 volts the thinner actuator has a maximum resonant free displacement just above 2 mm, while the shorter, wider actuator has a

maximum resonant free displacement of just under 1 mm. These values are approximately 5.8 times larger than the displacement at 1Hz. This is as expected because resonance magnifies the amplitude of vibrations in relatively undamped systems anywhere from 5 to 10 and sometimes 20 times over that of non-resonant vibrations.[30]

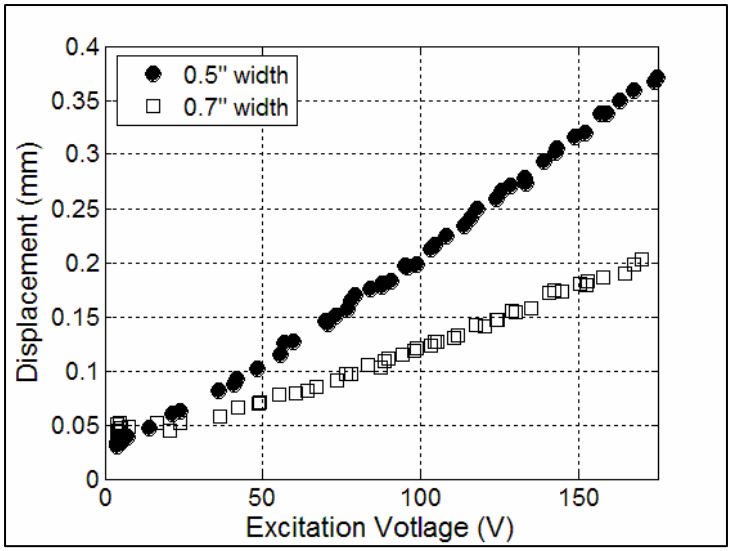

Figure 4.4 Free Displacement at 1 Hz with varying excitation voltage.

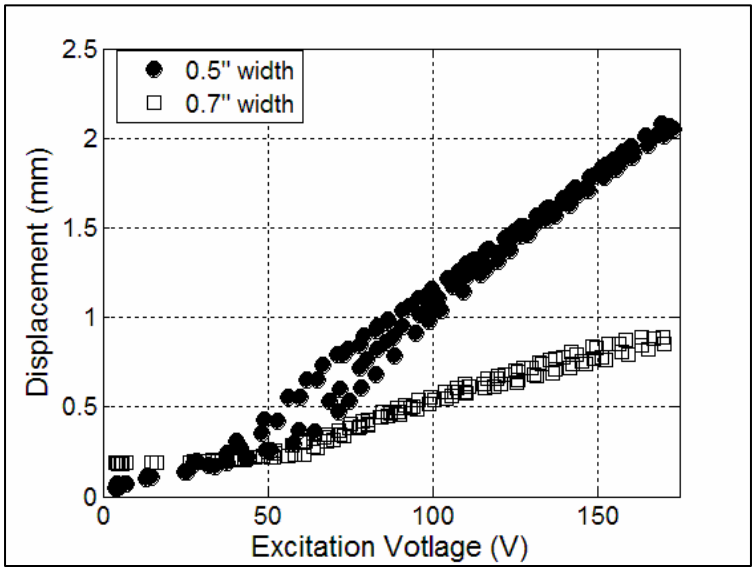

Figure 4.5 Free Displacement at resonance with varying excitation voltage.

After the free displacement tests were completed block force data was collect for both actuators. The method of calculating blocked force data will be discussed in detail in Chapter 5. Experimentally, the blocked force is found by collecting two points, one at zero load and one at an intermediate load. These two points are used to extrapolate the blocked force. Based on the dimensions of the piezo, the shorter, wider actuator should produce more moment and in turn, have a larger blocked force. This notion is supported by the data collect and represented in Figure 4.6. This figure shows the blocked force at 100 V_{pp} and 200 V_{pp}. The absolute blocked force most likely occurs at a voltage higher than 200 V_{pp} but in order to make sure the sample didn't depole, 200 Vpp was the maximum tested.

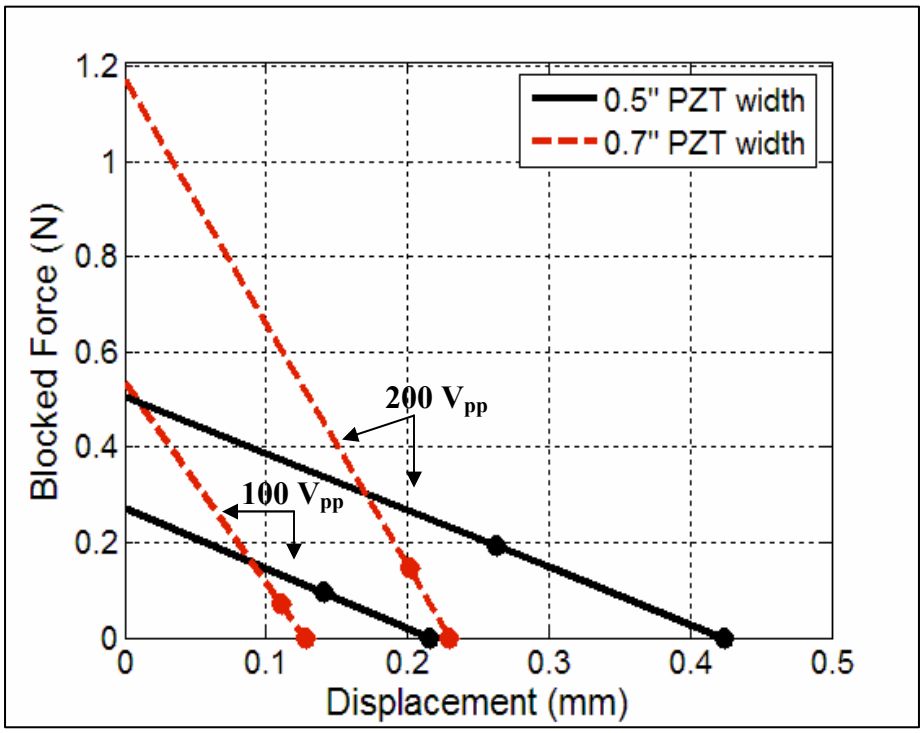

Figure 4.6 Blocked force at 100 V_{pp} and 200 V_{pp}.

Once free displacement data and blocked force was taken, both actuators were attached to the piston and latex membrane and chamber pressure, piston displacement and jet velocity data was taken. For these tests the larger chamber and piston were used (see Chapter 2) with a slot size of 1.143 mm x 17.78 mm. A plot of the piston displacement is shown in Figure 4.7.

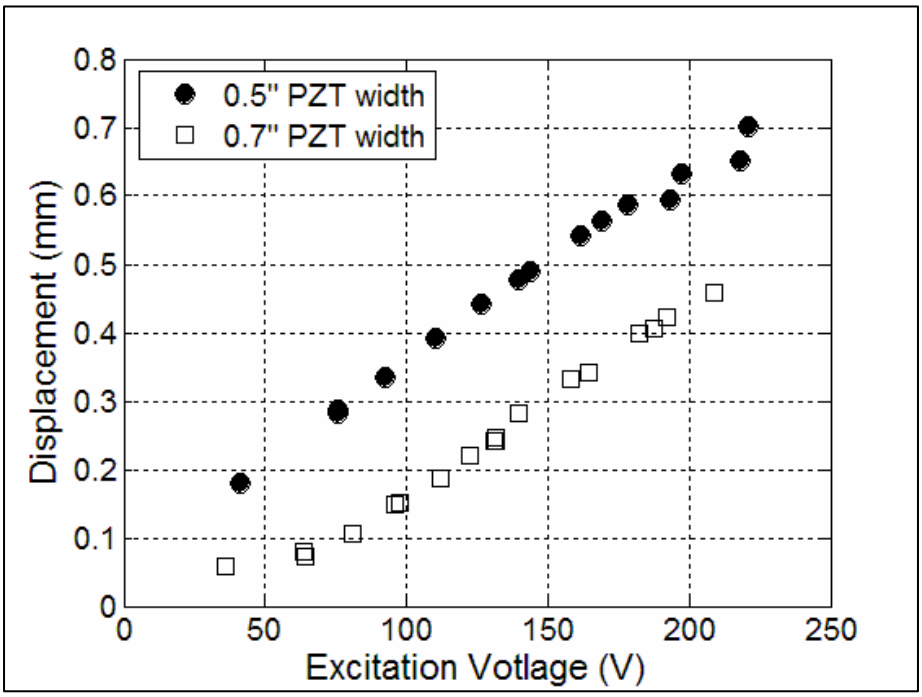

Figure 4.7 Piston displacement with varying excitation voltage.

The plot shows that the 0.5" actuator provides more piston displacement than the 0.7" actuator does. This is expected because the effective actuator stiffness of the narrower actuator is less than that of the larger actuator. The less stiff actuator will exhibit a greater displacement per unit force. The plot also shows that the slopes of the data are very similar. The slope of the 0.5" actuator data is 2.8e-3 mm/V while

the slope of the 0.7" actuator data is 2.5e-3mm/V. This is only an 11% difference. Given the same voltage, the piston displacement from the 0.5" actuator is on average .186 mm larger than the piston displacement from the 0.7" actuator.

As done in the test where the slot length was varied, chamber pressure data and velocity output data were taken for both synthetic jets. These results are shown in Figures 4.8 and 4.9.

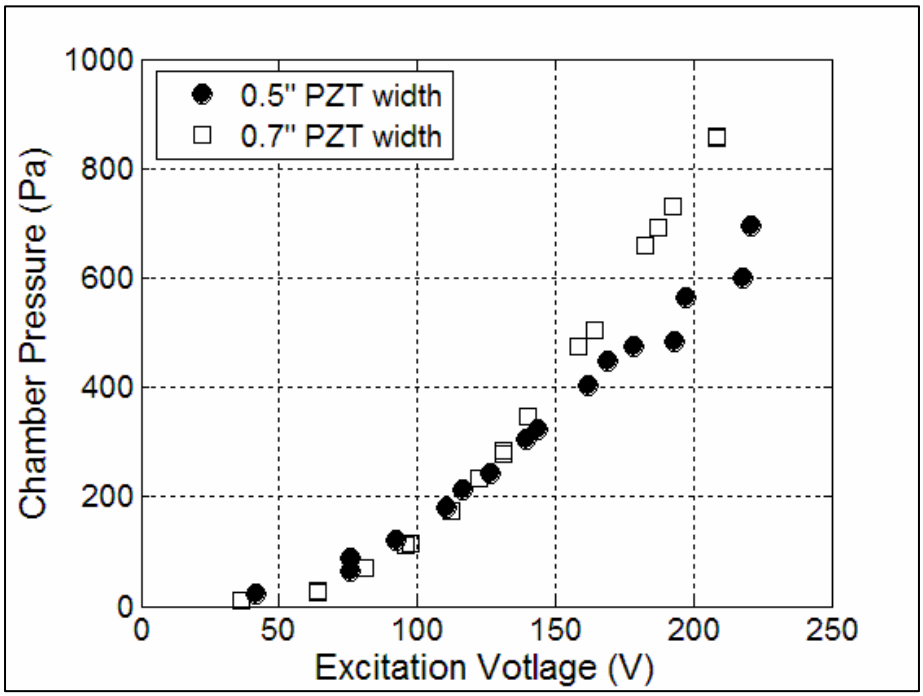

Figure 4.8 Chamber pressure with varying excitation voltage.

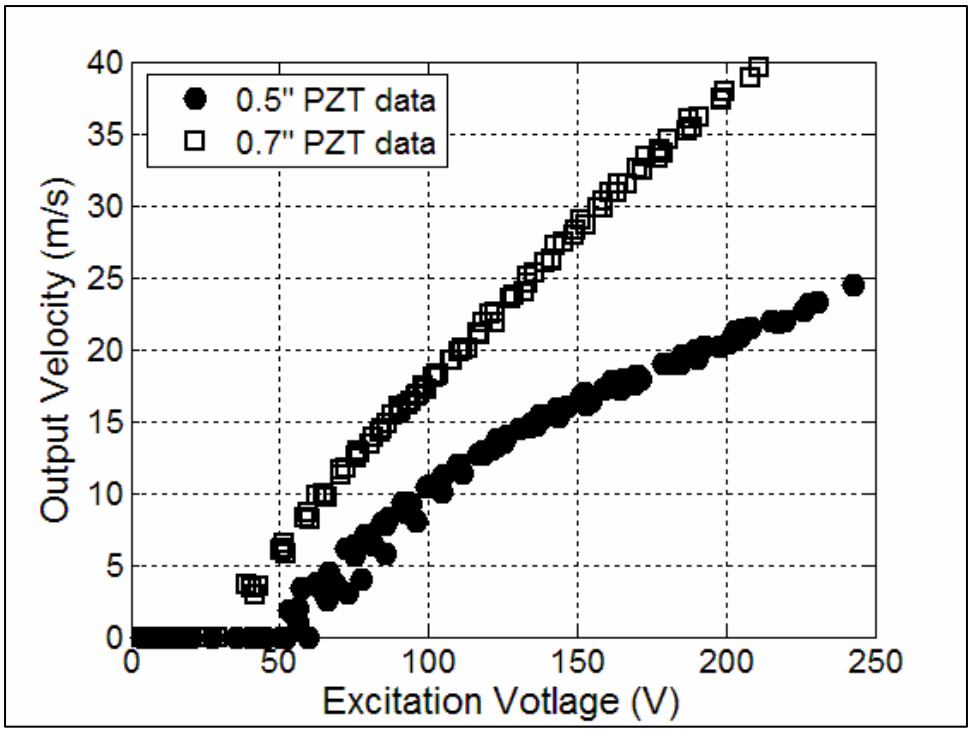

Figure 4.9 Output velocity with varying excitation voltage.

The plot shows that below 50 V_{pp} there us almost no velocity output. This is due to that fact that at the lower voltages, all of the displacement is used to pick up the extra slack in the latex so no air is being pushed out. In addition, the velocity of the 0.7" is higher than the jet velocity of the 0.5" actuator for all voltages. This is the same trend that is predicted by the model that will be discussed in further detail in Chapter 5.

Chapter 5: Synthetic Jet Model

While the synthetic jet was being built and tested, a fellow graduate student was working on developing a model of the synthetic jet.[25] The model consists of two parts coupled together to form the full model. The first is the motor model and the other is the fluid model. Figure 5.1 shows a schematic of the model.

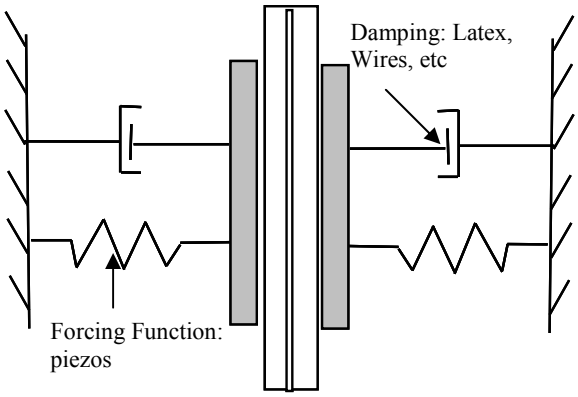

Figure 5.1 Schematic of synthetic jet model.

5.1 Motor Model

The motor model is simply a spring-mass-damper system. Euler Bernoulli beam theory is used to determine the flexural stiffness of the bimorph and the moment induced by the change in piezo layer length. This leads to a transverse displacement. Once the displacement is known the blocked force can be solved for.

The beam used to model the actuators is an isotropic beam with symmetric surface bonded actuators. Equations 5.1 and 5.2 show how the flexural stiffness, EI_{tot}, and

bending moment, M_Λ, of the beam are calculated using the Euler-Bernoulli beam model:

$$EI_{tot} = \sum E_i b_i (h_{i+1}^3 - h_i^3) \tag{5.1}$$

$$M_\Lambda = \sum \Lambda_i E_i b_i (h_{i+1}^2 - h_i^2) \tag{5.2}$$

where E_i is the stiffness of the ith layer, b_i is the width of the ith layer, Λ_i is the free strain of the ith layer, and h_i is the vertical position of the interface between two different layers.[29] Figure 5.2 shows a schematic of a layered beam such as the one used the one used in the model. The Figure shows the definition of each h_i.

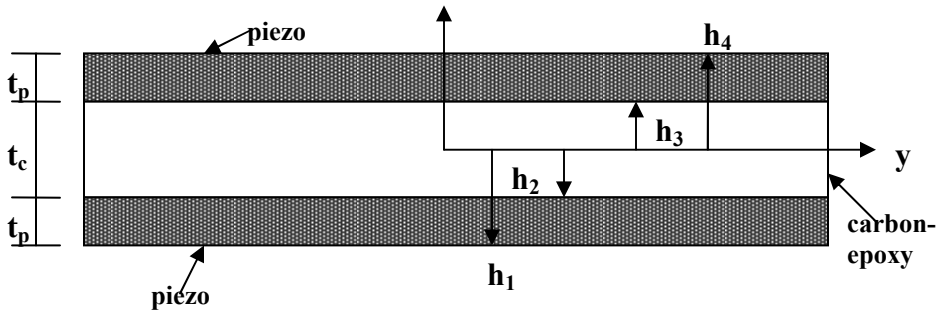

Figure 5.2 Isotropic beam with symmetric surface bonded actuators.

When the top and bottom piezos are actuated at equal but opposite voltages the actuator is in pure bending. This means that the piezo with a negative applied voltage results in a negative actuation strain and the positive voltage results in a positive actuation stain. This is shown in Figure 5.3.

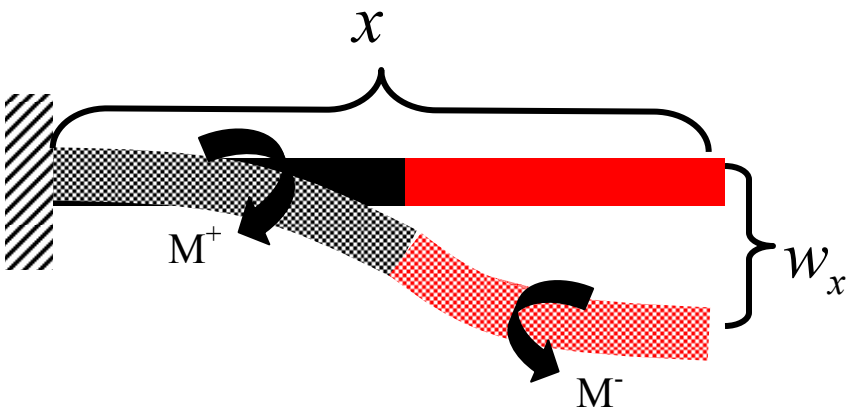

Figure 5.3 Symmetric beam in pure bending.[29]

Once the moment and flexural stiffness are calculated, the displacement can be calculated using equation 5.3,

$$w_x = \frac{Mx^2}{EI} \tag{5.3}$$

where x is the position on the beam and w_x is the transverse displacement at the location x. When modeling the recurve actuator used in this thesis, x is located at $L/4$, the point where electrodes are etched off. To determine the total displacement of the synthetic jet w_x is multiplied by four. This is because there are two sections on each actuator that displace equal amount (they have equal but opposite moments) and each synthetic jet contains two actuators.

In order to determine the blocked force of the synthetic jet we must employ the clamped-clamped boundary conditions. The displacement of a clamped-clamped beam with a point load at *L/2* is a well documented value. It is a function of force, flexural stiffness, and beam length. Because we already know the displacement of the beam, we can solve the equation for force. This force is the blocked force, shown in equation 5.4.

$$F_{blk} = \frac{192EIw_{L/2}}{(L/2)^3} \tag{5.4}$$

Once the blocked force is known it, along with the displacement, are used as inputs into the fluid model in order to predict the performance of the synthetic jet.

5.2 Fluid Model

The fluid model describes the flow into and out of a synthetic jet. It is a function of piston force and displacement, the chamber, slot, and piston size, and the properties of the air. The model was developed specifically for synthetic jets by Clingman.[25] A schematic of the fluid section of the model is shown in Figure 5.4.

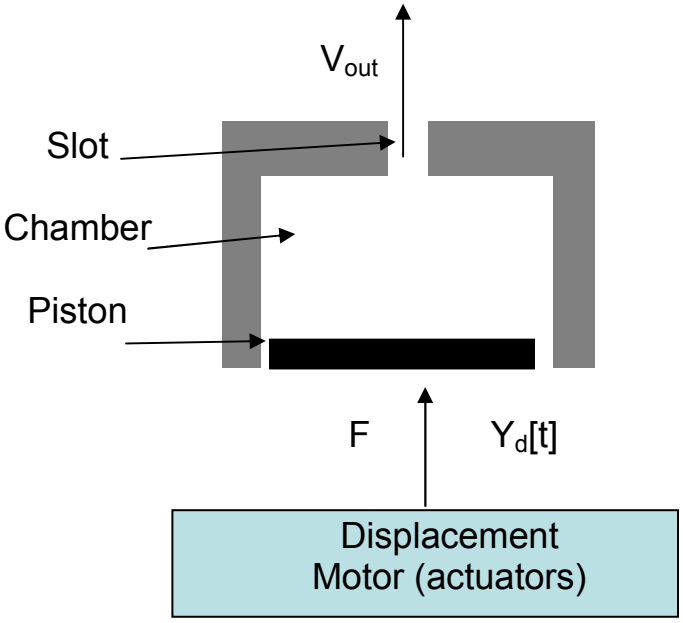

Fluid Model States

m_a	Air mass in chamber
T_c	Temperature in chamber
p_a	Pressure in chamber
Y_d	Piston displacement

Fluid Model Parameters

A_s	Slot area
A_p	Piston area
V_{ac}	Initial chamber area
T_a	Outside air temperature
p_{atm}	Atmospheric pressure
R	Air gas constant
ã	Ratio of Cv/Cp

Figure 5.4 Schematic of fluid model.[25]

The model assumes an adiabatic process where there is no heat flow in or out of the system. In addition, the model accounts for other losses by the use of a dimensionless slot loss coefficient that could vary from 0 to 1. A value of 1 assumes there are no losses. In order to match the model to the experimental data, slot loss coefficients

ranging from .029 to 0.4 were used for the 0.5" actuator and slot loss coefficients ranging from .047 to 0.68 were used for the 0.7" actuator.

In the model, Clingman[25] solves for the derivatives of the chamber states: the air mass in the chamber, temperature in chamber, and pressure in chamber. The result is three nonlinear differential equations for air mass, chamber pressure, and chamber temperature. These are shown below in equations 5.5, 5.6 and 5.7:

$$\frac{dm_a}{dt} = -\rho A_s k_s \sqrt{p_a - p_{atm}} \tag{5.5}$$

$$\frac{dp_a}{dt} = \frac{\rho A_s \sqrt{p_a - p_{atm}} RT_c}{V} - P_a \frac{dV}{dt} - \frac{p_a R \frac{dV}{dt}}{C_v V} \tag{5.6}$$

$$\frac{dT_c}{dt} = -\frac{p_a \frac{dV}{dt}}{C_v m_a} \tag{5.7}$$

where ρ is the air density, A_s is the area of the slot, k_s is the slot loss coefficient, P_a is the air pressure inside the chamber, P_{atm} is the atmospheric pressure, R is the gas constant, T_c is the temperature inside the chamber, V is the air volume of the chamber, and m_a is the mass of the air in the chamber. Solving for P_a with time leads to the jet velocity in equation 5.8.

$$V_{out} = k_s \sqrt{\frac{P_a - P_{atm}}{\rho_{air}}} \tag{5.8}$$

5.3 Experimental vs. Model Comparison

Estimates of the free displacement and blocked force are only functions of the motor model and don't require taking into account any fluid interactions. The free displacement data taken at 1 Hz as well as the modeled free displacement are show in Figures 5.5 and 5.6.

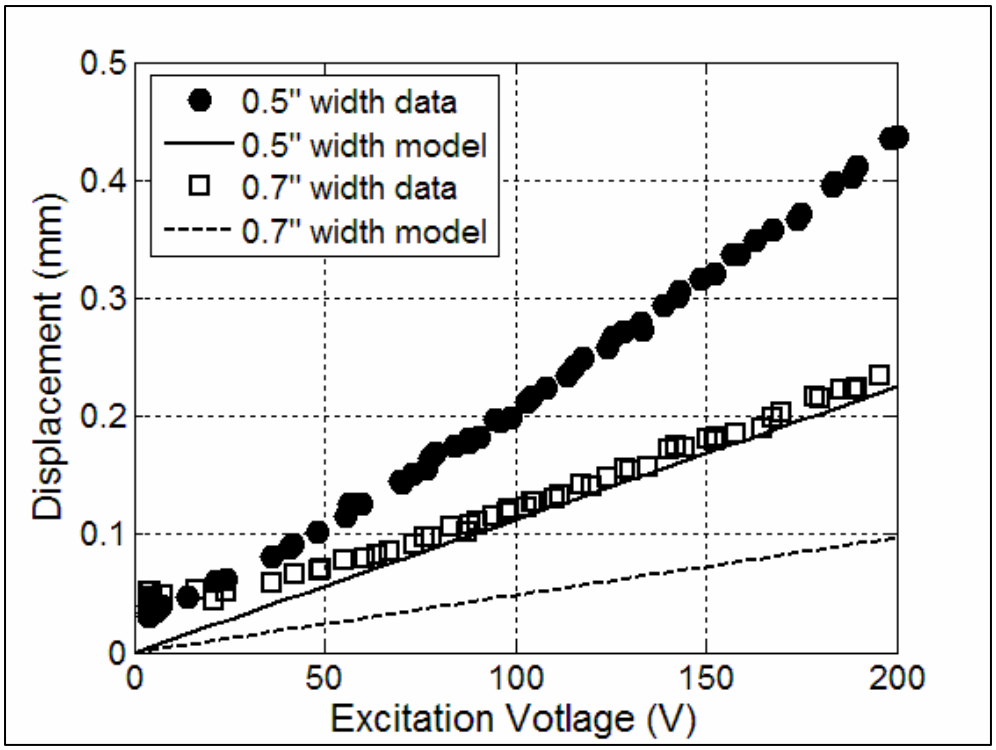

Figure 5.5 Displacement with varying excitation voltage as modeled.

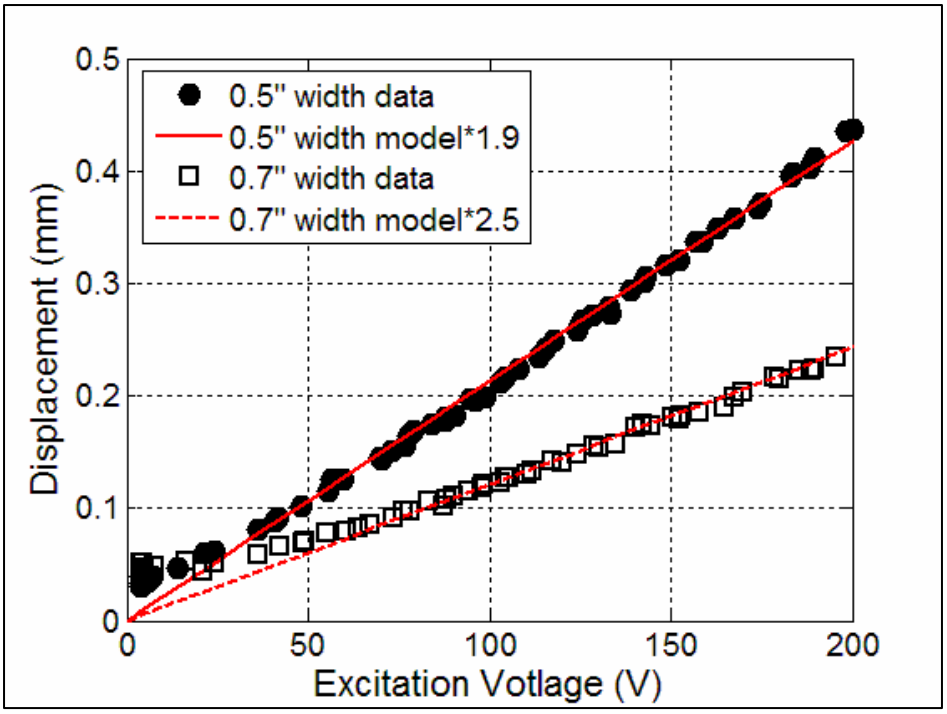

Figure 5.6 Displacement with varying excitation voltage performance predictions scaled by a factor of 1.9 and 2.5 for the 0.5" and 0.7" actuators respectively.

The plot shows that the experimental data outperforms the model. The 0.5" actuator performs 1.9 times better than the model and the 0.7" actuator performs 2.5 times better than the model. This is represented in figure 5.6 by the modeled lines which have steeper slopes than the modeled lines on figure 5.5. One possible cause of this is that the actual stiffness of the experimental actuator is less than the modeled value. The model assumes perfect bonds between the piezo and the carbon/epoxy. Perfect bonds result in a stiffer actuator. Although great care was taken to compress the piezos before curing, there is no guarantee that the bonds were perfect.

The lowest voltage that was tested was 4 volts. The plots show that at these voltages the displacement is about 0.03 mm. However, if the lower voltages were to follow the same linear trend as the rest of the data the values should be almost a magnitude less at about 0.003mm. As will be discussed later in this section, these actuators tend to exhibit non-linear behavior at lower voltages but this not does not explain why the starting point seems to be higher than it should be. One thought is that there may have been a DC offset which was unaccounted for. If this was the case, all of the data would need to be shifted down 0.025 mm. However, if this were done, the modeled data would only be valid for voltages greater than 50 volts. This is shown in figure 5.7.

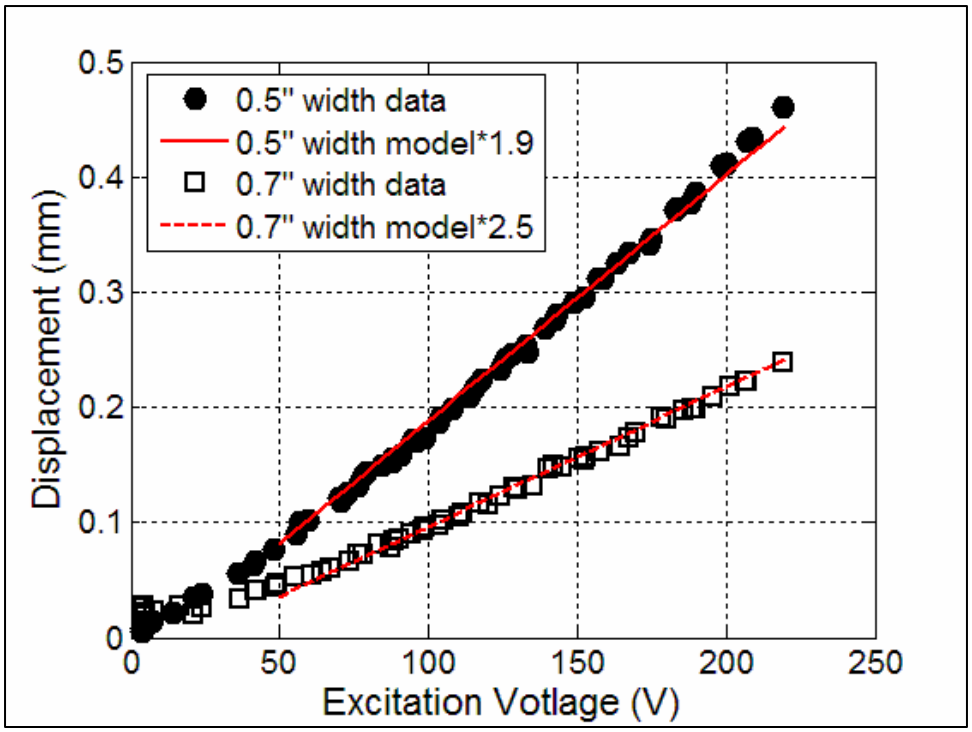

Figure 5.7 Shifted displacements with varying excitation voltage

Figure 5.8 shows the blocked force data as well as the modeled blocked force. As mentioned in the previous section, the model shows that the 0.7" actuator's blocked force should be greater than the 0.5" actuator's blocked force. The data agrees with this. In fact, the model under-predicts the blocked force for the 0.7" actuator. In addition, it over-predicts the blocked force for the 0.5" actuator but only by a small amount.

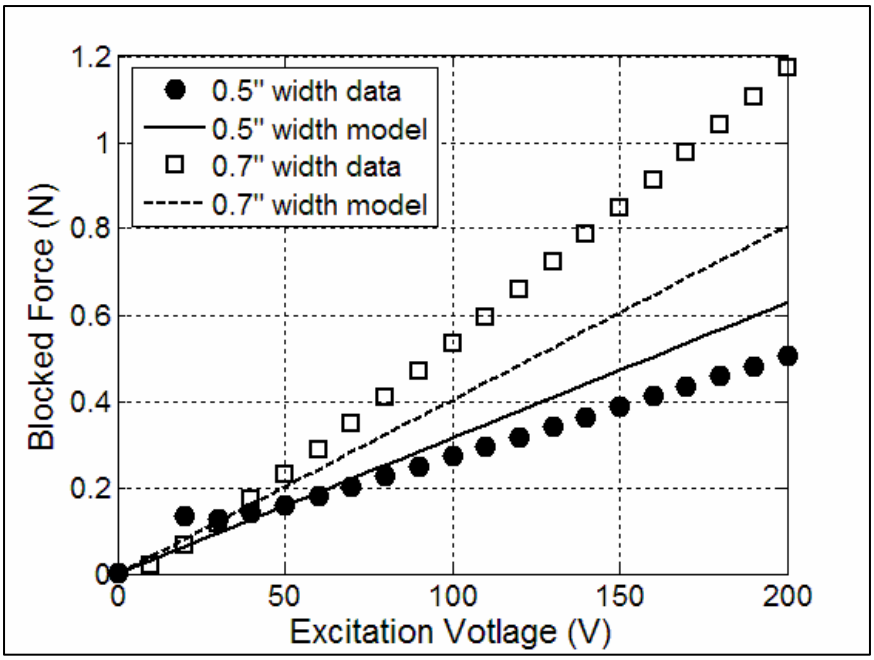

Figure 5.8 Blocked force with varying excitation voltage.

In addition to the slot loss coefficient, there is a damping coefficient used to adjust the modeled data to better match the experimental data. The damping coefficient and the slot loss coefficient are chosen to force the model to match the displacement and velocity output as closely as possible. The damping coefficient was set such that the displacement matched the experiential data. The damping coefficient was 0.0185 for

the 0.5" actuator and 0.0173 for the 0.7" actuator. These values are very typical of damped systems such as these.

As stated previously, in order to match the model to the experimental data slot loss coefficients ranging from .029 to 0.4 were used for the 0.5" actuator and slot loss coefficients ranging from .047 to 0.68 were used for the 0.7" actuator. These loss coefficients imply an "efficiency" of the synthetic jet. For these two synthetic jets the 0.7" actuator was more efficient then 0.5" actuator; however; the losses incurred but the synthetic jet are very highly dependant on the alignment of the actuator, piston, latex and chamber. Even the slightest twist in the latex can have a dramatic effect on the velocity output. For these two specific cases it is most likely that the piston had better alignment when connected to the 0.7" actuator. In addition, one cannot assume that these loss coefficients will be same for all synthetic jets.

One final assumption that was made before matching the displacement and velocity data was in regards to the stiffness of the actuator, *EI*. The model assumes perfect bonds and thus and ideal stiffness. However it is very unlikely the actuators had perfect bonds. In fact, the free displacement and blocked force data discussed above validate the assumption that the stiffness of the actuators was less than the ideal stiffness. Thus, a stiffness coefficient was used to scale the stiffness down. As with the slot loss and damping coefficients, many values were tested and in the end a stiffness coefficient of 0.9 was determined to be the best fit. This was the case for

both actuators. Once all the coefficients were determine the modeled data matched the experimental data very well.

Figure 5.9 compares the experimental piston displacement of the 0.5" and 0.7" actuators with the modeled piston displacement. The piston displacement is the displacement of the actuator when it is working against the latex and with the mass of the piston. For the 0.5" actuator the average difference is only 2.27%. This is slightly lower and the average percent difference for the 0.7" actuator. It's mean percent difference was 13.5%.

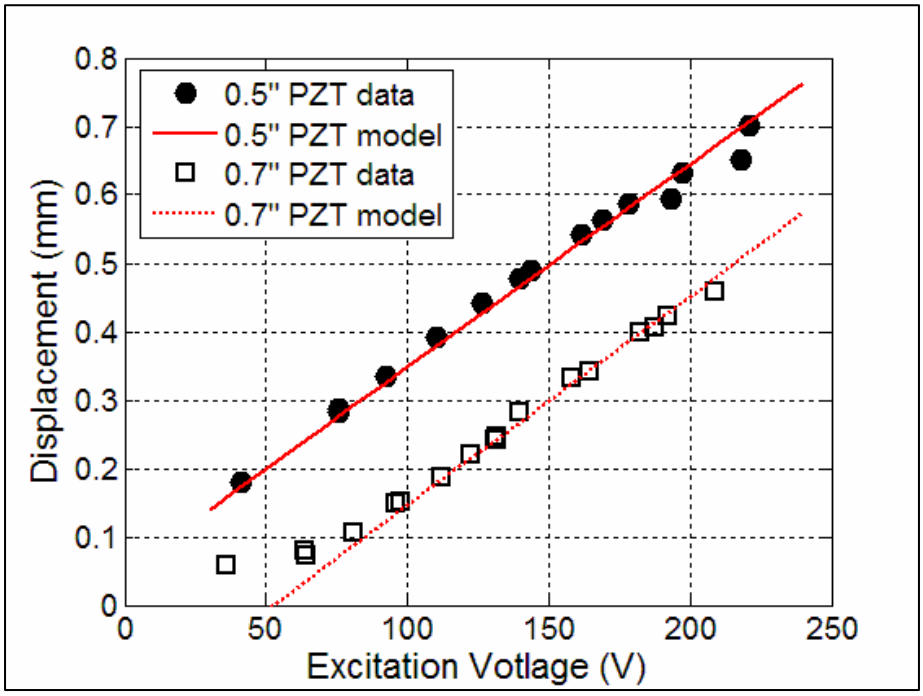

Figure 5.9 Displacement with varying excitation voltage.

Finally, the velocity output data collected from both the 0.5" and 0.7" actuators was compared to the model. The results are shown in Figures 5.10. Both sets of data

match the model well. As predicted by the model, the velocity output of the 0.7" actuator out performs the 0.5" actuator. As mentioned in the previous section, below 100 V_{pp} almost all of the piston displacement (work) is being used to pick up slack in the latex. The efficiency at these lower voltages is extremely low; thus, the plot only shows the velocity output for voltages above 100 $V_{pp.}$ The plot shows that even above 100 V_{pp} the efficiency steadily increased with increased voltage.

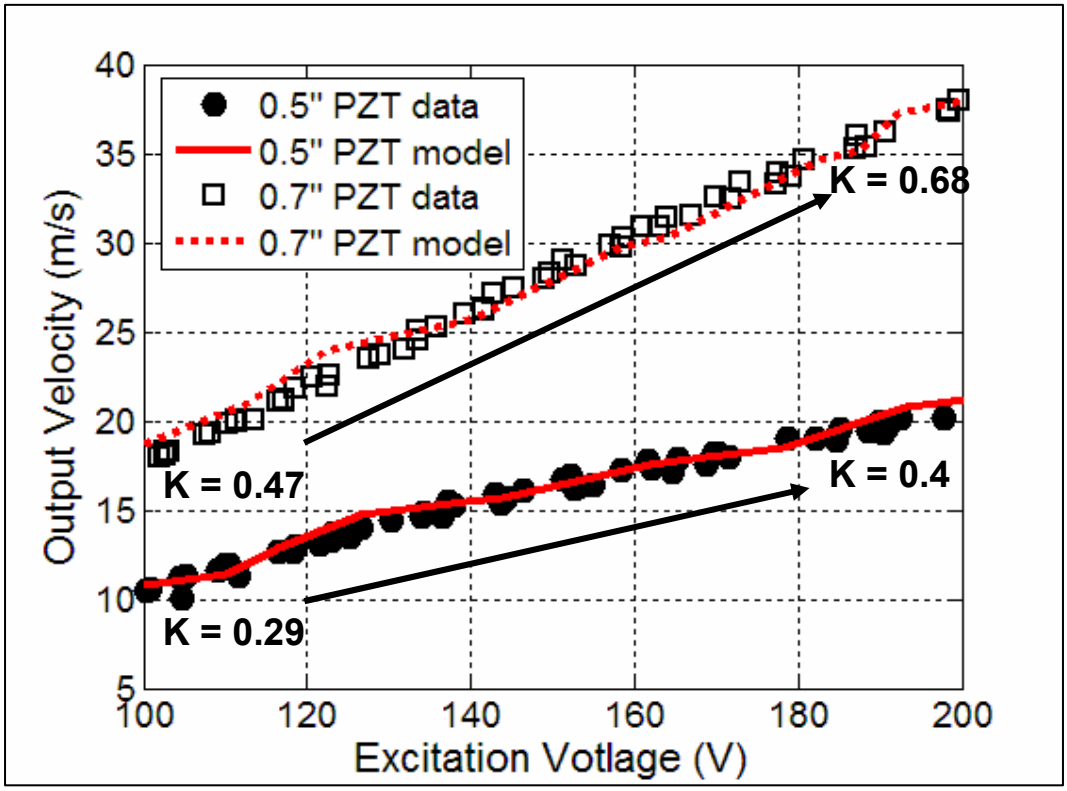

Figure 5.10 Output velocity with varying excitation voltage.

Chapter 6: Flow Visualization

Flow visualization tests were run in order to get a feel for how the synthetic jet affects the flow field. The tests were meant to give only a basic understanding of the flow and not necessarily meant to fully characterize the flow field. This chapter will discuss the experimental set-up of the visualization test as well as the results.

6.1 Smoke/Laser Set-up

The set-up consists of a six-jet atomizer for smoke generation, a wind tunnel rake for smoke to flow through, and a laser with a glass wand to make the smoke visible. Figure 6.1 shows the six-jet atomizer used for the smoke generation. There are three switches that can be turned on or off in order to alter the amount of smoke generated. This in turn, alters the velocity at which the smoke exits the rake.

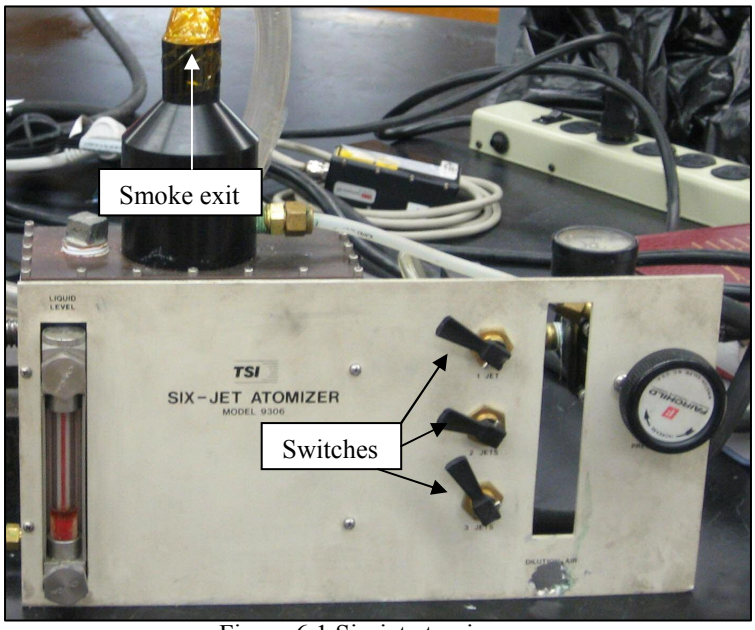

Figure 6.1 Six-jet atomizer.

The rake was used to straighten the flow. The total height of the rake is 25.5 cm. There are 25, 3-cm long prongs through which the smoke exits. The prongs are each 1 cm apart. The rake, along with its dimensions, is shown in Figure 6.2. Figure 6.3 shows the laser along with the glass wand.

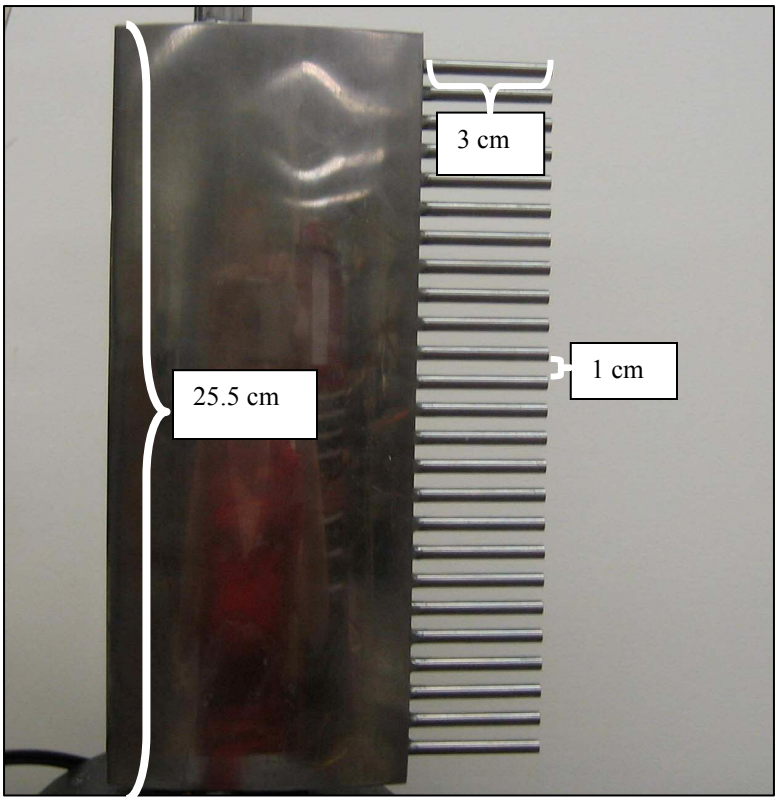

Figure 6.2 Wind tunnel rake.

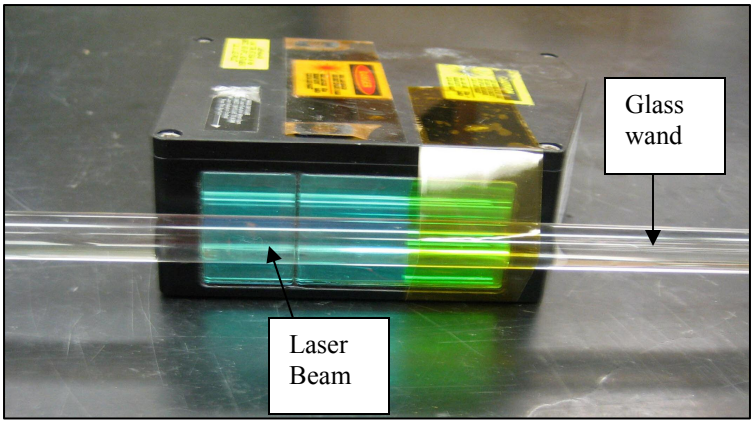

Figure 6.3 Laser and glass wand.

Figures 6.4 and 6.5 show plots of the complete set-up. Figure 6.4 is the set-up with the lights on and Figure 6.5 shows how the laser makes the smoke visible in the dark.

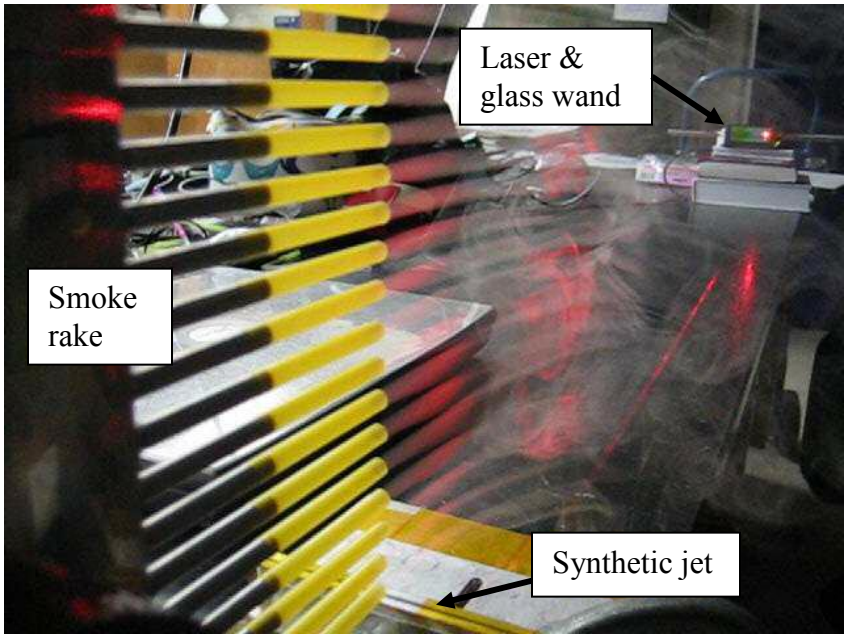

Figure 6.4 Complete set-up with lights on.

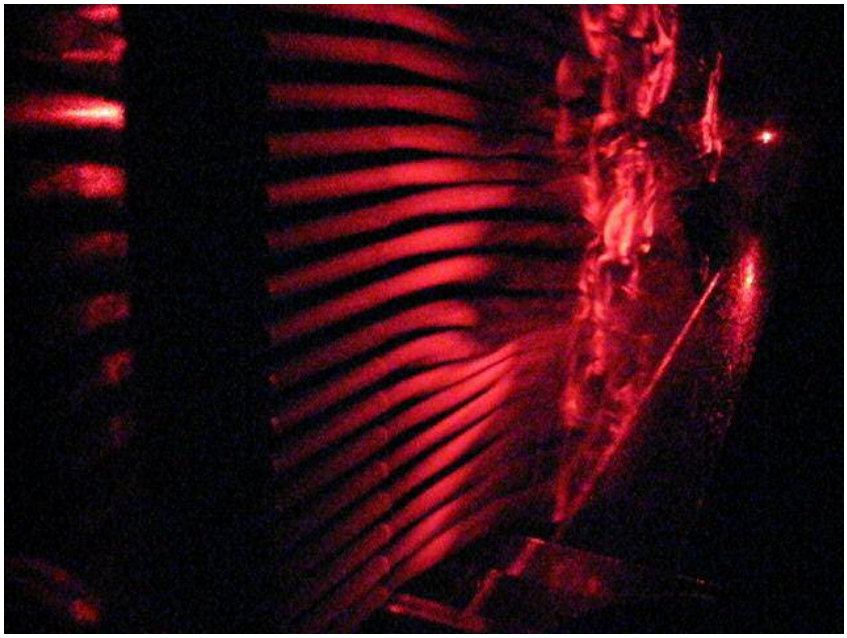

Figure 6.5 Complete set-up with lights off.

6.2 Visualization Results

The flow patterns were observed at two different jet speeds and three cross-flow speeds. The synthetic jet speeds were 13 m/s and 6.5 m/s and the cross flow speeds were 15 m/s, 7 m/s and less than 1 m/s. The synthetic jet was run at it's natural frequency, 147 Hz. The distance between vorticies can be calculated by using equation 6.1:

$$d = \overline{U}_{jet} / \omega_n \tag{6.1}$$

where d is the distance between the vorticies, $\overline{U}_{jet}$ is the mean synthetic jet velocity and ω_n is the frequency used to generate the jet (147 Hz in this case). For the case when the synthetic jet velocity is 6.5 m/s the vorticies should be approximately 2.3 cm apart and when the synthetic jet velocity is 13 m/s the vorticies should be about 4.87 cm apart.

Figures 6.6, 6.7 and 6.8 show the flow for a synthetic jet velocity of 6.5 m/s at each of the three cross-flows. The figures show that for all three cross flows the vortices are right around where they should be. The average error between the calculated and observed is only 5.6%. The major difference between the three figures is the amount that the jet penetrates the cross flow. As expected, we see that at the lowest cross flow velocity the jet penetrates the flow field at a much higher angle than at the two larger cross flow velocities. Because the pictures are taken at an angle it is difficult to determine an exact angle but when compared to each other there is a noticeable relative difference.

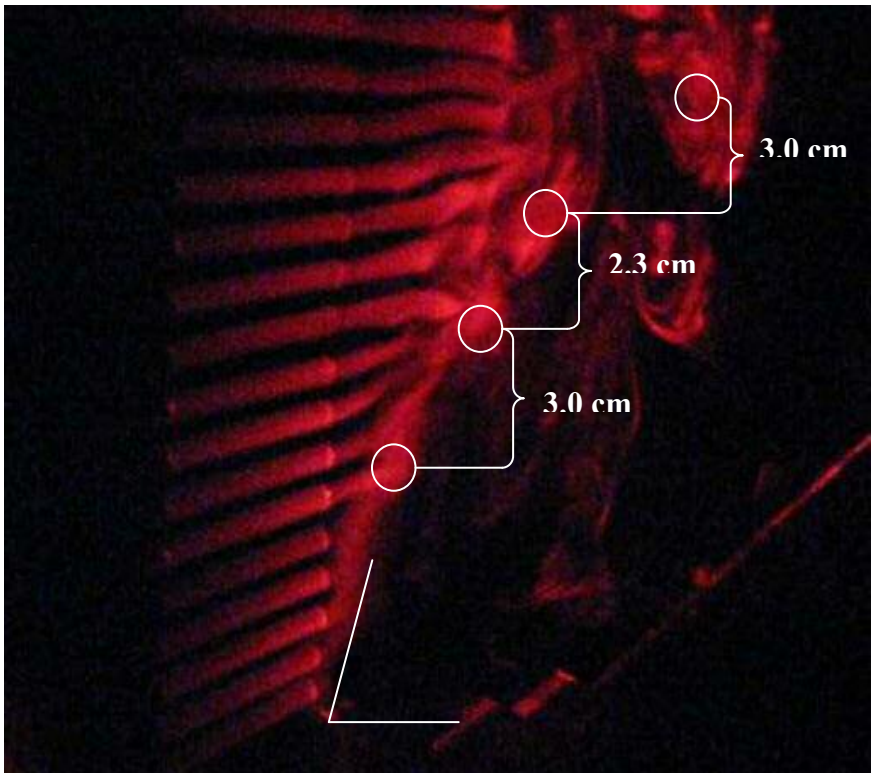

Figure 6.6 Flow with < 1m/s cross flow and 6.5 m/s jet velocity.

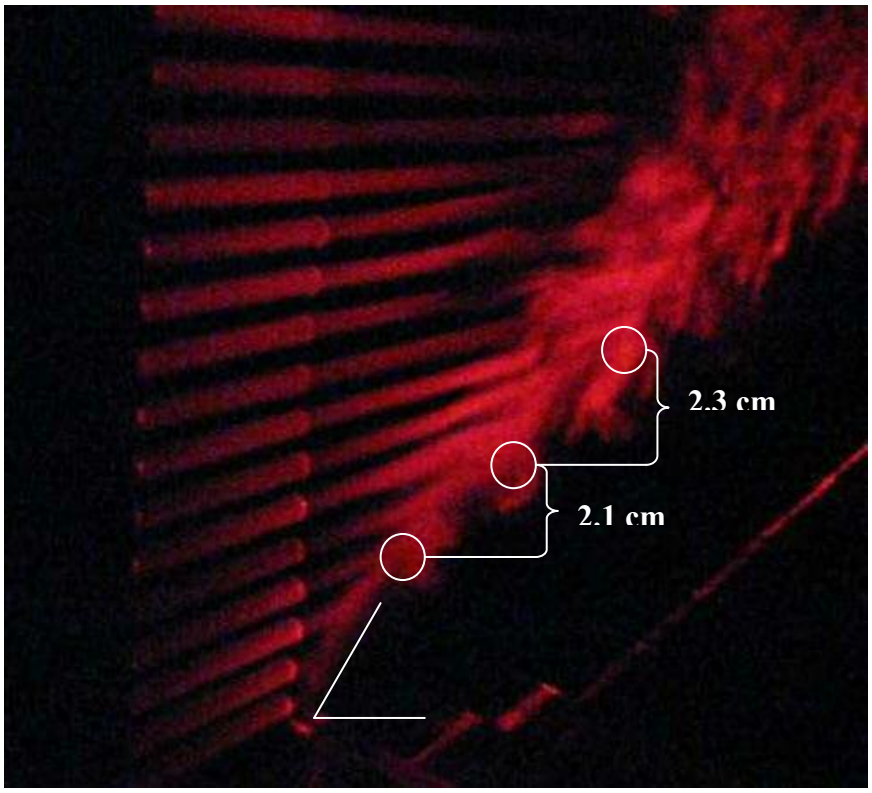

Figure 6.7 Flow with 7m/s cross flow and 6.5 m/s jet velocity.

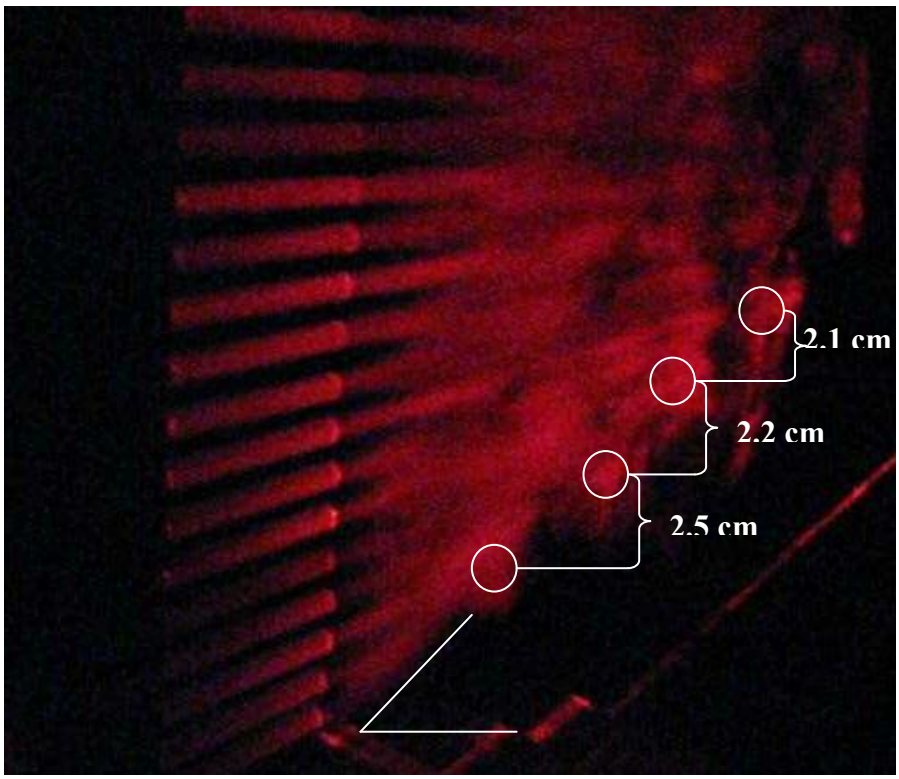

Figure 6.8 Flow with 15 m/s cross flow and 6.5 m/s jet velocity.

The second jet velocity that was observed was 13 m/s. Figures 6.9, 6.10, and 6.11 show this flow at each of the three cross flows. As with the smaller jet velocities, the vorticies are spaced where they should be. According to calculations, the distance between the vorticies should be 4.87cm apart. The observed distances are on average, 15% different that the calculated distances. As with the photos taken at the 6.5 m/s cross flow, the major difference in the three flows is the amount that the jet penetrates cross flow. Again, as expected, the jet penetrates the lower cross flow at a much higher angle than it does at the higher cross flow.

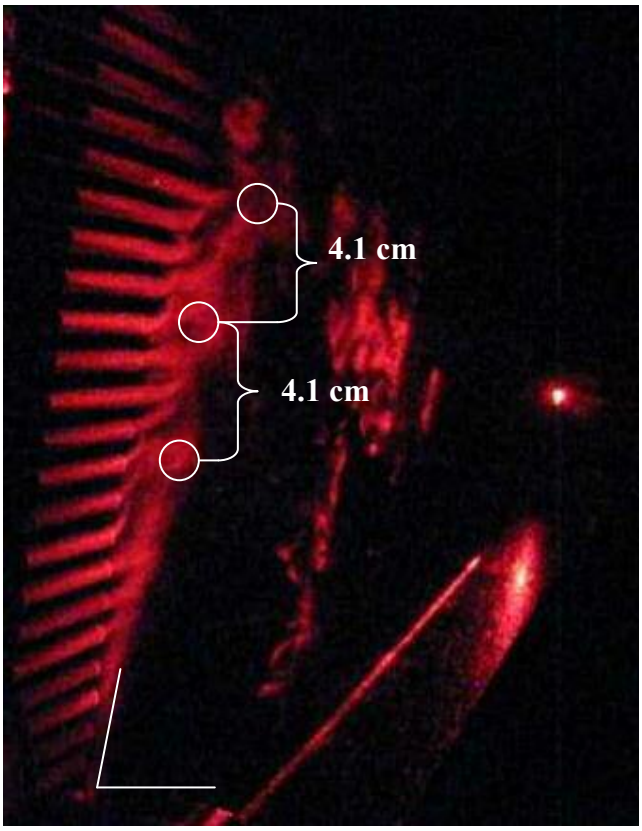

Figure 6.9 Flow with <1 m/s cross flow and 13 m/s jet velocity.

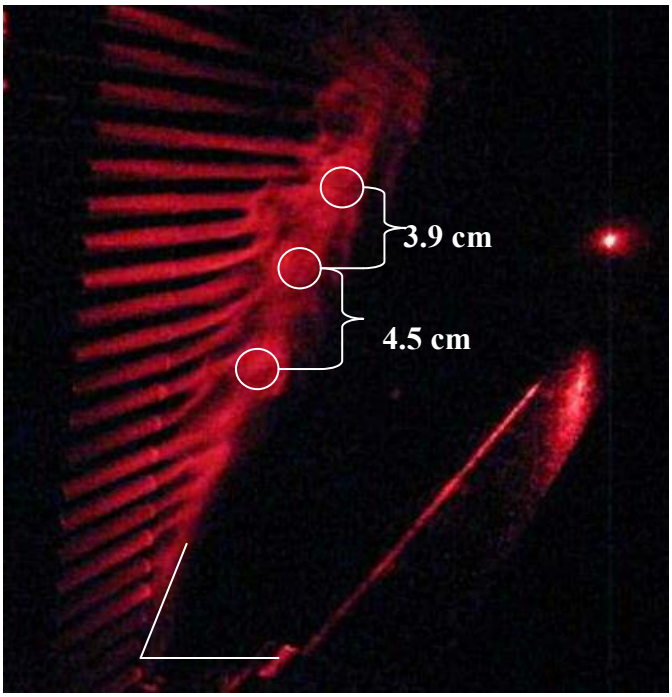

Figure 6.10 Flow with 7 m/s cross flow and 13 m/s jet velocity.

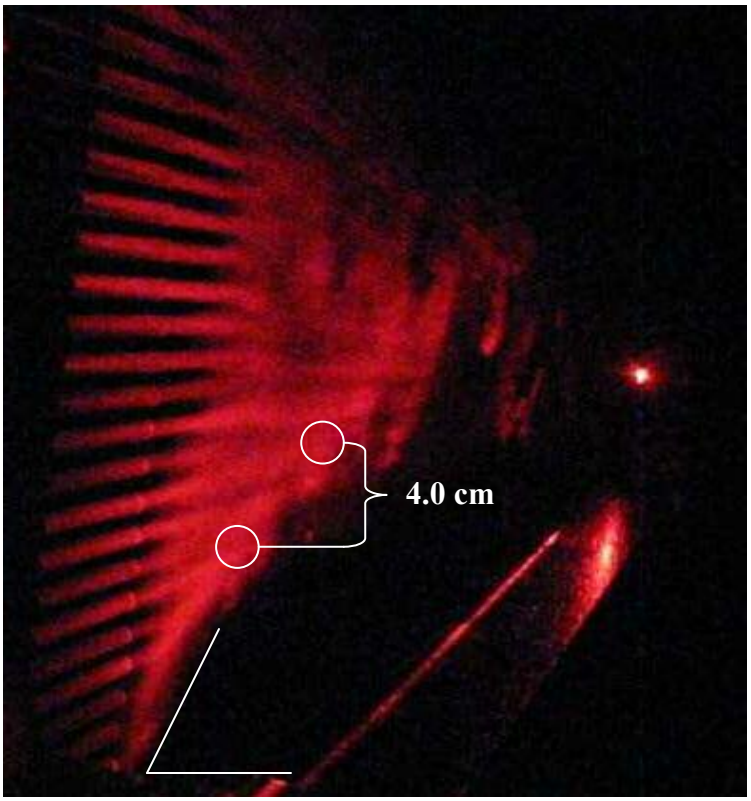

Figure 6.11 Flow with 15 m/s cross flow and 13 m/s jet velocity.

Chapter 7: Conclusions and Future Work

The initial goals of the study have been met. Our design of a lightweight low frequency actuator has met our expectations and is competitive with other actuators and synthetic jets currently being developed. This is shown is Tables 2 and 3.

Actuator	Mass	Free Displacement
UMD actuator	14.6 g	3.0 mm
*LIPCA C-1	4.9 g	0.17 mm
**THUNDERTM 7-R (1/3)	7.3 g	0.08 mm

*Yoon, K.J, Kyungpook National University **US patent 5632841

Table 2. Comparison of low mass, smart material-based actuators

Synthetic Jet	Displacement	Velocity Output	Endurance
UMD actuator	1.5 mm	13 m/s	over 1B cycles
***PVDF Bender	3.5 mm	15 m/s	≈ 20M cycles

***Calkins, F.T, Boeing

Table 3. Comparison of low mass, smart material-based synthetic jets

These tables show that while the UMD actuators weigh about twice that of other actuators being developed, they provide one to two orders of magnitude more displacement. Furthermore, when we compare the fully constructed synthetic jet to others being developed we find that we slightly less displacement, similar velocity output, and endurance that is three orders of magnitude more than the endurance of the PVDF synthetic jet currently being investigated. These results are very promising and it is believed that further study and fine-tuning of the design will provide even more displacement and velocity output at an even lower overall mass.

We have also shown the effect of changing the chamber slot size on synthetic jet velocity output. Slot sizes ranging from 1.27 mm to 73.66 mm can produce velocity outputs anywhere from 30 m/s to 13 m/s. This is a fairly wide range of velocities and shows that these actuators can be used for a many different applications. When a lot of control is needed over a small surface area the smallest slot size can be used and when less control is needed over a larger surface the same actuator can be used with just a small modification to the slot size.

We have also been able to conclude that modifying the geometric shape of the piezo bimorph has a significant effect on the velocity output of the synthetic jet. In fact, at 200 V_{pp} the 0.7" synthetic jet can achieve 34 m/s out of the slot while the 0.5" synthetic jet can only get 25 m/s. Simply changing the shape of the original design, while maintaining the same mass and amount of active material, increased the velocity output by 30%. In both cases, by just altering the voltage, the velocity output can be reduced or increased to meet the flow control needs.

Finally, we have shown the performance of the UMD synthetic jet matches Clingman's synthetic jet model very well when given the correct coefficients. This allows us to use the model to determine a relative efficiency of the synthetic jet. With this model relative efficiencies of 40% and 68% were found for the 5" and 7" synthetic jet actuators respectively. It also shows that we have the ability to model different synthetic jet configurations to see which actuator, chamber and slot sizes

perform better before they are built. This can save both time and money in the long run.

While this research led to many relevant and important results concerning the design of synthetic jet actuators for use active flow control, there is still a lot for future work that can be done. Endurance is one of the most important factors that must continue to be tested. If these synthetic jets are ever to be put on an aircraft they need to be proven to stand the test of time. While reaching 1 billion cycles is a huge milestone, it is desirable that they last tens of billions of cycles. In addition, multiple actuators need to undergo such endurance tests.

One undesirable effect of the endurance test was the drift in the natural frequency. One way to make the endurance tests more efficient would be to have the actuator sense small changes in it's displacement and automatically adjust it's frequency. This can easily be done using a program such as Labview.

Finally, devising a more reliable means of attaching the leads to the piezos is desirable. Leads coming off of the piezos was the main problem encountered throughout this research. While this problem was easily solved by simply re-soldering the leads, a more reliable method is desired.

These above suggestions represent near term modification to the existing experimental set-up; however, there is also a lot of future work that can be done

which involves bringing the resonance based synthetic jet actuator concept to a new level for future MS and PhD students. This study has developed a baseline concept. Integration of this concept into a wing is a vital step in the research and development of this technology. Studied that look at lift and drag profiles will provide valuable information as to how the jets perform in aerodynamic conditions. Also, there are numerous possible trade studies that can and should be done. For example, it would be very valuable to know how multiple synthetic jets in cross flow interact with each other. In addition, creating a single jet that can alter it's slot size and angle would allow the effect of the synthetic jet to change with changing flight conditions.

This research has been fun and interesting and has introduced many new ideas into the world of active flow control. First, based on an extensive literature search, no one has looked at a bi-morph PZT actuator for use in active flow control. This new idea showed that this approach can produce much more output than current configurations at only a slightly larger weight. Also, this project was the first to test the PLZT-98 for use in a synthetic jet. The results of these tests are the first known data regarding the large displacement potential of this new material. Lastly, the most valuable contribution this project has made to the smart materials and active flow control community is the endurance test results. Endurance tests with other actuators tend to make it to a couple million cycles before failure of the piezo material. The fact that this design made it to a billion cycles without any failure in the PZT is truly remarkable and valuable result.

Appendix

Displacement data was taken for all of the actuators using the Microtrak II Laser Triangulation Senor made by MTI Instruments Inc. The sensor is very easy to use because it gives a digital readout that is can be sent directly to a data system with very little calibration. The voltage signal only needs to be multiplied by 0.1 to convert the displacement from volts to inches. Figure A.1 show a picture of the Microtrak II displacement sensor.

Figure A.1 Microtrak II laser displacement sensor.[26]

A 5-inch H_2O pressure sensor was used to measure chamber pressure as well as velocity output. The operating range is -10 to +10 psig. Figure A.2 shows what the sensor looks like.

Figure A.2 Schematic of pressure sensor.

Before the sensor could be used it had to be calibrated. This was done by simply connecting the sensor to a small hose that was connected to a pipette. Water was added in half inch increments and data was taken. The calibration plot as well as the calibration equation can be seen below in Figure A.3

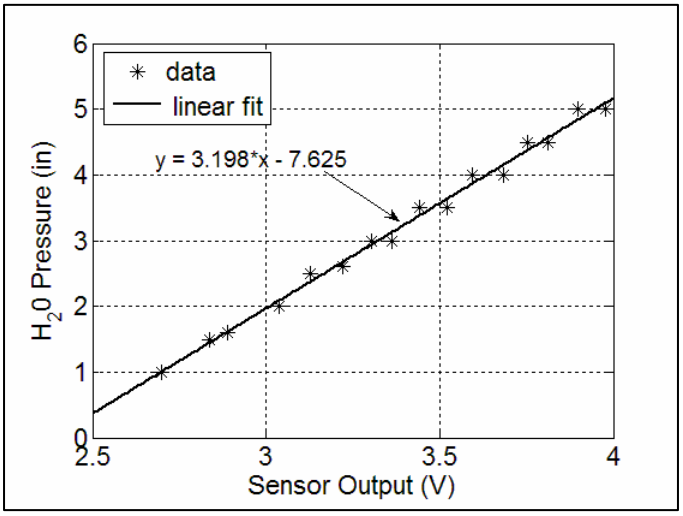

Figure A.3 Pressure sensor calibration plot.

Block force data was collected using a beam load cell with a 0.2 lb capacity. Figure A.4 shows a picture of the load cell.

Figure A.4 Picture of Futek bending beam load cell.

Like the pressure sensor, the load cell had to be calibrated before it could be used. This was done my hanging masses in 5 gram increments of the end of the load cell and measuring the voltage output. By converting the masses into forces a voltage output vs. force calibration plot was created. This is shown in Figure A.5.

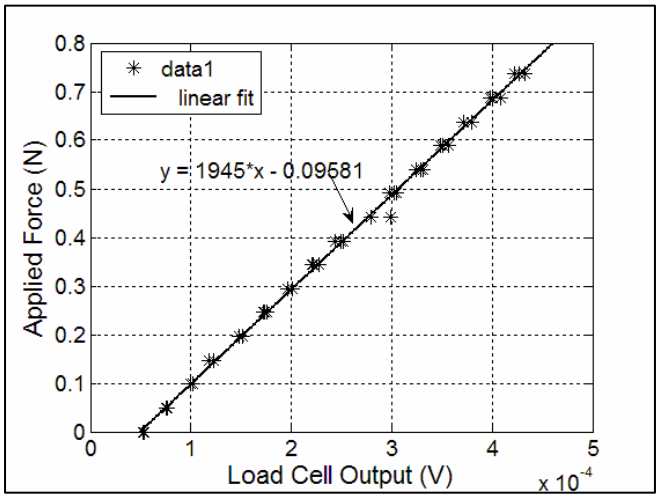

Figure A.5 Load cell calibration plot.

References

1. L. Pack, R. Joslin. "Overview of Active Flow Control at NASA Langley Research Center. SPIE 3326. 1999. pg 202-213.

2. D. Greenblatt, I. Wygnanski. "The Control of Flow Separation by Periodic Excitation". Progress in Aerospace Engineering Vol 36. 2000. pg 487-545.

3. S. Mallinson, J. Reizes, G. Hong, M. Buttini. "Synthetic Jet Actuators for Flow Control". SPIE 3891. 1999.

4. M. Chandrasekhara, M. Wilder, L. Carr. "Unsteady Stall Control Using Dynamically Deformed Airfoils". AIAA Journal, Vol 36, Issue 10. 1998.

5. F. Collins, J. Zelenevitz. "Influence of Sound Upon Separated Flow Over Wings". AIAA Journal, Vol 13, Issue 3. 1975. pg 408-410.

6. K. Bremhorst, P.G. Hollis. "Velocity Field of an Axisymmetric Pulsed, Subsonic Airjet". AIAA Journla, Vol 28. 1990. pg. 2043-2049.

7. K. McManus, J. Magill. "Airfoil Performance Enhancement Using Pulsed Jet Separation". AIAA paper 01-5632

8. A. Siefert, A. Darabi, I. Wygnanski. "Delay of Airfoil Stall by Periodic Separation". AIAA Journal of Aircraft, Vol 33 No 4. July 1996. pg 691-698.

9. K. Bailo, D. Brei, F. Calkins. "Investigation of PVDF Active Diaphragms for Synthetic Jets". *Proceedings of SPIE* Vol. 3991. 2000.

10. F. Calkins, J. Mabe, J. Smith, D. Arbogast. "Low Frequency (F^+ =1.0) Multilayer Piezopolymer Synthetic Jets fit Active Flow Control". AIAA vol 2823. 2002.

11. Q.C. Xu, A. Dogan, J. Tressler, S. Yoshikawa, R. E. Newnham. "Ceramic-metal Composite Actuator". *IEEE Ultrasonics Symposium*. 1991. pg 923-928.

12. R. E. Newnham, A. Dogan, Q.C. Xu, K. Onitsuka, J. Tressler, S. Yoshikawa. "Flextensional "Moonie" Actuators". *IEEE Ultrasonics Symposium*. 1993. pg 509-513

13. F. Lalande, Z. Chaudhry, C. A. Rogers. "A Simplified Geometrically Nonlinear Approach to the Analysis of the Moonie Actuator". *IEEE Trans. Ultason. Ferroelct. And Freq. Cont*., Vol 42, No 1. 1995. pg. 21-27.

14. S. Dong. "Ring Type Uni/BiMorph Piezoelectric Actuators". *Journal of Intelligent Material Systems and Structures*, Vol 12. 2001. pg. 613-616.

15. G. H. Heartling. "Rainbow Ceramics – A New Type of Ultra-High-Displacement Actuator". *American Ceramic Society Bulletin*, Vol 73, No 1. 1994. pg. 93-96.

16. S. A. Wise. "Displacement Properties of RAINBOW and THUNDER Piezoelectric Acuators". *Sensors and Actuators*, Vol 69. 1998. pg. 33-38.

17. J. Juutu, E. Heinonen, V. Moilanen, S. Leppavuori. "Displacement, Stiffness and Load Behavior of laser-cut RAINBOW Actuators". *J. Euro. Ceram. Soc.*, Vol 24. 2004. pg. 1901-1904/

18. S.A. "Thunder Rolls In". *Mechanical Engineering*, Vol 118, Issue 12. pg. 14.

19. http://www.prestostore.com/cgi-bin/pro23.pl?ref=thunderonline&pg=17412

20. K.M. Mossi, R.P. Bishop. "Characterization of Different Types of High Performance THUNDER Actuators". *SPIE*, Vol 3675. 1999. pg 43-52.

21. K. Yoon, S. Shin, H. Park, N. Goo. "Design and Manufacture if a Lightweight Piezo-composite Curved Actuator". Smart Materials and Structures 11. 2002. pg 163-168.

22. K. Kim, K. Park, H. Park, N. Goo, K. Yoon. "Performance Evaluation of Lightweight Piezo-composite Actuators". Sensors and Actuators, A 120. 2005. pg 123-129.

23. J. Ervin, D. Brei. "Recurve Piezoelectric-Strain-Amplifying Actuator Architecture". *IEEE/ASME Trans on Mechatronics*, Vol 3, No 4. 1998. pg 293-301

24. F. T. Calkins, J.H. Mabe. "Multilayer PVDF Actuator for Active Flow Control". AIAA Paper 2001-1560. 2001.

25. D. Clingman. "Development of an Aerodynamic Synthetic Jet Based on a Piezoceramic Buckled Beam". Master Thesis University of Maryland. 2006.

26. http://www.directindustry.fr/prod/mti-instruments/capteurs-de-position-laser-19330-48755.html

27. http://www.allsensors.com/datasheets/J2/AmpLow/amp_low.pdf

28. http://www.futek.com/hires.asp?product=FP10025%2D00013%2DC&model=L1501&title=+bending+beam+load+cell

29. I. Chopra. ENAE 51 Smart Structures class notes. Fall 2004

30. http://www.update-intl.com/VibrationBook2a.htm

31. T.C. Corke, M.L. Post. "Overview of Plasma Flow Control: Concepts, Optimization, and Applications". AIAA paper # 2005-563.

32. C.L Enloe, E.J. Jumper. "Mechanisms and Responses of a Dielectric Barrier Plasma". AIAA Papae # 2003-1021.

33. N.S. Goo, C. Kim, Y, Kwon, K. Yoon. "Behaviors and Performance Evaluation of a Lightweight Piezo-Composite Curved Actuator". Journal of Intelligent Material Systems and Structures, Vol 12. Sept 2001. pg 639-645.

34. S. Mallinson, G. Hong, J. Reizes. "Fundamental Studies of a Synthetic Jet Actuator". 13th Australian Fluid Mechanics Conference. 1998.

35. F. Calkins, D. Clingman. "Vibrating Surface Actuators for Active Flow Control". The Boeing Company. 2003.

36. B. Smith, A. Glezer. "The formation and evolution of Synthetic Jets". Physics of Fluids, Vol10 No 9. Sept 1998. pg 2281-2297.

37. A. Jacot, J. Mabe. "Boeing Active Flow Control for the V-22". AIAA Fluids 2000. June 2000.

38. A. Honohan, M. Amitay, A. Glezer. "Aerodynamic Control Using Synthetic Jets". AIAA Fluids 2000. June 2002. AIAA 2000-2401.